The Astrophysical Journal Supplement Series, 159:314–330, 2005 August

THE ELECTRON EXCITED ULTRAVIOLET SPECTRUM OF HD: CROSS SECTIONS AND TRANSITION PROBABILITIES

Joseph Ajello and Prahlad Vatti Palle[1]
Jet Propulsion Laboratory, California Institute of Technology, Pasadena, CA 91109

Hervé Abgrall and Evelyne Roueff
LUTH and UMR 8102 du CNRS, Observatoire de Paris, 92195 Meudon Cedex, France

Anil Bhardwaj[2]
NASA Marshall Space Flight Center, Space Science Branch, NSSTC/XD12, Huntsville, AL 35805

and

Jacques Gustin
University of Liège, Liège, Belgium
Received 2004 July 9; accepted 2005 April 19

ABSTRACT

We have analyzed the high-resolution ultraviolet (UV) emission spectrum of molecular deuterium hydride (HD) excited by electron impact at 100 eV under optically thin, single-scattering experimental conditions. The high-resolution spectrum (FWHM = 160 mÅ) spans the wavelength range from 900 to 1650 Å and contains the two Rydberg series of HD: $^1\Sigma_u^+ 1s\sigma$, $np\sigma(B, B', B'', n = 2, 3, 4) \rightarrow X\,^1\Sigma_g^+$ and $^1\Pi_u^+ 1s\sigma$, $np\pi(C, D, D', D'', n = 2, 3, 4, 5) \rightarrow X\,^1\Sigma_g^+$. A model spectrum of HD, based on newly calculated transition probabilities and line positions including rovibrational coupling for the strongest band systems, $B\,^1\Sigma_u^+$–$X\,^1\Sigma_g^+$, $B'\,^1\Sigma_u^+$–$X\,^1\Sigma_g^+$, $C\,^1\Pi_u$–$X\,^1\Sigma_g^+$, and $D\,^1\Pi_u$–$X\,^1\Sigma_g^+$, is in excellent agreement with observed intensities. The cross sections for direct excitation at 100 eV of the $B\,^1\Sigma_u^+$, $B'\,^1\Sigma_u^+$, $C\,^1\Pi_u$, and $D\,^1\Pi_u$ states were derived from a model analysis of the experimental fluorescence spectrum to the ground state. The absolute cross section values for excitation to the $B\,^1\Sigma_u^+$, $B'\,^1\Sigma_u^+$, $C\,^1\Pi_u$, and $D\,^1\Pi_u$ states were found to be $(2.57 \pm 0.26) \times 10^{-17}$, $(0.22 \pm 0.06) \times 10^{-17}$, $(2.54 \pm 0.25) \times 10^{-17}$, and $(0.17 \pm 0.04) \times 10^{-17}$ cm^2, respectively. We have also determined the dissociative excitation cross sections at 100 eV for the emission of Lyα at 1216 Å and Lyβ at 1025 Å lines, which are $(7.98 \pm 1.12) \times 10^{-18}$ and $(0.40 \pm 0.10) \times 10^{-18}$ cm^2, respectively. The summed excitation function of the closely spaced pair of lines, H Lyα and D Lyα, resulting from dissociative excitation of HD, has been measured from the threshold to 800 eV and is analytically modeled with a semiempirical relation. The model cross sections are in good agreement with the corrected Lyα cross sections of Möhlmann et al. up to 2 keV. Based on measurements of H, D ($2s$) production cross section values by Möhlmann et al., the H, D ($n = 2$) cross section is estimated to be 1.6×10^{-17} cm^2 at 100 eV.

Subject heading: molecular data

1. INTRODUCTION

1.1. *Astrophysics and the Solar System*

The primordial abundance of the deuterium element, D, is continually depleted in the cosmos by nuclear processes within the interior of stars. The study of D abundance by HD ultraviolet (UV) absorption techniques has far-reaching cosmological significance as the present HD abundance is a lower limit to the primordial abundance (Ferlet et al. 2000). HD is the third most abundant molecule in the interstellar medium (ISM). The *Copernicus* satellite detected interstellar HD via UV absorption transitions, belonging to the Lyman and Werner electronic band systems, toward bright stars (Spitzer et al. 1973) such as Zeta Ophiuchi (Morton 1975). More recently, with the *Far Ultraviolet Spectroscopic Explorer* (*FUSE*) satellite, a sample of these HD UV absorption transitions has also been detected in a variety of interstellar translucent clouds toward less bright stars in the Galactic and extragalactic environments (Ferlet et al. 2000; André et al. 2004; Lacour et al. 2005; Boissé et al. 2005). The analysis of the *Copernicus* interstellar data is based upon the HD wavelengths measured by Dabrowski & Herzberg (1976) and the transition probabilities calculated by Allison & Dalgarno (1970). The shortcomings of these values based on Hönl-London factors for molecular hydrogen and its isotopes have been pointed out by Liu et al. (1995) and Abgrall et al. (1999). Allison & Dalgarno (1970) band transition probabilities partitioned by Hönl-London factors yield significant errors when nonadiabatic rovibronic correction and centrifugal potential are not negligible. The nonadiabatic correction mainly affects close-lying levels.

In the solar system HD has been observed in the atmosphere of all four giant planets (Jupiter, Saturn, Uranus, and Neptune), with an HD/H_2 abundance ratio of $(1-10) \times 10^{-5}$ (Taylor et al. 2004). The determination of the D/H ratio in the giant planets has long been recognized as a powerful tool to understand the formation of the solar system from the primitive nebula. The H Lyα line is one of the strongest lines in the spectrum of the giant planets' aurora (cf. Bhardwaj & Gladstone 2000), mainly produced through electron impact dissociative excitation of H_2 gas in their upper atmospheres. However, some contribution to this auroral line from the outer planets' atmospheres can also

[1] Present address: Institute for Plasma Research, Bhat, Gandhinagar 382428, India.

[2] On leave from Space Physics Laboratory, Vikram Sarabhai Space Centre, Trivandrum 695022, India.

come from dissociative excitation of HD, whose contribution is not known. Even observation of the D Lyα line from Jupiter's airglow has been reported (Ben Jaffel et al. 1998), although it has been contested too (Parkinson et al. 1999). The possibility exists for the presence of HD in the extrasolar giant planets. Indeed, H Lyα has been detected in absorption toward HD 209458b (Vidal-Madjar et al. 2003), which is a Jupiter-like planet orbiting a Sun-like star, indicating the presence of H and H_2 in its atmosphere. Finally, we mention the detection of D-bearing molecules (HDO and DCN) in comets, where the D/H abundance ratio, in HDO/H_2O, is estimated to be $\sim 3 \times 10^{-4}$ (Bockelée-Morvan et al. 2005). This ratio can be used to infer the processing a comet has undergone during evolution to estimate the pristine nature of its nucleus content. Interestingly, the D/H ratio in comets is about twice the terrestrial value and about a factor of 10 higher than the values found in the protosolar material, but quite similar to that found in the interstellar medium, which may indicate a similar origin.

1.2. *Molecular Physics*

Electron impact collision processes on HD have been studied both experimentally and theoretically. Geiger & Schmoranzer (1969) investigated the electron energy loss spectra of HD at 34 keV and measured the integrated vibrational intensities of the Lyman and Werner bands. Geiger & Schmoranzer (1969) determined Franck-Condon factors and isotope effects among H_2, HD, and D_2. Dissociative recombination processes for specific vibrational states of HD^+ have been measured by Amitay et al. (1999). Core excited resonances in HD, for the 11–13 eV electron energy range, have been studied by Furlong & Newell (1995). On the theoretical side, rotational excitation of HD by low-energy electrons has been calculated by Hara (1971), and vibrational excitation of HD has been analyzed theoretically by Kazanskii (1996). More recently, Celiberto et al. (2001) created an extensive theoretical database for the electron impact inelastic cross sections of HD, emphasizing the dissociative electron attachment cross sections at very low energies (less than 6 eV).

Electron impact dissociative excitation cross sections of HD have been studied experimentally via the analysis of the Lyα emission arising from principal quantum number $n = 2$, H, D ($2p$, $2s \rightarrow 1s$ transitions) through the processes

$$e + \mathrm{HD} \rightarrow \mathrm{H} + \mathrm{D}^* + e \rightarrow \mathrm{H} + \mathrm{D} + h\nu + e$$
$$\rightarrow \mathrm{H}^* + \mathrm{D} + e \rightarrow \mathrm{H} + h\nu + \mathrm{D} + e.$$

These cross sections were measured at electron energies of 100–2000 eV by the group from Holland (Möhlmann et al. 1978) about 25 years ago. Their measurements were based on the pre-1985 value of cross section of the H Lyα from dissociative excitation of H_2 at 100 eV of 1.2×10^{-17} cm^2, compared to the more recent and accurate value of 7.16×10^{-18} cm^2 (Liu et al. 1998). Moreover, due to experimental constraints, the measurements of Möhlmann et al. (1978) are limited to energies $\geq$100 eV, and therefore no information is available on the threshold and near-threshold region. Additionally, Ajello et al. (1991, 1995a, 1995b) have shown that the dissociation of H_2 molecules proceeds by branches for singly and doubly excited states. The set of dissociation reactions for the H Lyα and the D Lyα (hereafter H, D Lyα) produced during dissociative excitation of HD can be identified using analytic models to fit the measured excitation function. To our knowledge the UV spectrum of HD under single-scattering conditions of electron impact fluorescence has not been measured before. Emission experiments in discharge tubes have been conducted in the past for determining rotational and vibrational constants (Dabrowski & Herzberg 1976). The laboratory measurements of emission cross sections are the basis to analytical models for calculations of electron energy loss in gaseous environments rich in hydrogen molecules and its isotopes (e.g., Singhal et al. 1992; Dalgarno et al. 1999; Ajello et al. 2005; cf. Bhardwaj & Gladstone 2000 and references therein). Reliable cross sections are obtained through coupling between laboratory program and theory (Liu et al. 1998).

1.3. *Plan for Paper*

We have recently reported the analysis of high-resolution UV emission spectra following electron impact excitation of H_2 (Liu et al. 1995, 2000; Jonin et al. 2000) and D_2 (Abgrall et al. 1999). The discrete and continuum line transition probabilities were calculated by Abgrall et al. (1993a, 1993b, 1993c, 1994, 1997) for H_2 and Abgrall et al. (1999) for D_2. In this paper we report a combined experimental and theoretical investigation of the UV emission spectrum of HD. The theoretical study involves detailed calculations of emission transition probabilities of individual rotational lines of the $B\ ^1\Sigma_u^+ - X\ ^1\Sigma_g^+$, $B'\ ^1\Sigma_u^+ - X\ ^1\Sigma_g^+$, $C\ ^1\Pi_u^+ - X\ ^1\Sigma_g^+$, and $D\ ^1\Pi_u^+ - X\ ^1\Sigma_g^+$ band systems. The experimental record is concerned with the measurement of high-resolution (0.16 Å FWHM) electron impact-induced UV emission spectra from 900 to 1700 Å. We have also measured the excitation function of the H, D Lyα produced in dissociative excitation of HD in the low- and medium-energy regions (10–800 eV) and made an estimate of the dissociative excitation cross sections of the HD Rydberg state for $n = 2$ and 3 at 100 eV.

The organization of the paper is as follows. Section 2 describes briefly the experimental apparatus used to measure the UV emission from the deuterium hydride molecule produced by electron impact. Section 3 reports the relative flow measurement of the H, D Lyα cross section at 100 eV. The coupled Schrödinger equations formalism used in ab initio calculations of continuum and discrete transition probabilities for the first two principal quantum number levels ($n = 2, 3$) of HD is related in § 4. In the model section (§ 5), we provide a concise description of the theoretical model used to analyze the observed electron impact fluorescence intensities, which takes into account the B, B', C, and D' states. In § 6, cross sections are determined for each of the B, B', C, and D states at 100 eV. Section 7 describes the analysis of the electron impact dissociative excitation cross sections for the combined optically allowed transition of H, D Lyα at 1215.67 and 1215.34 Å, respectively. Section 8 is a summary section and discussion of the results.

2. EXPERIMENTAL APPARATUS

The experimental setup, which consists of an electron–molecular-beam collision chamber and a 3 m UV spectrometer interfaced for computer control and data acquisition, has been described in previous papers (Liu et al. 1995; Ajello et al. 1995a, 1995b, 1996; Jonin et al. 2000; Vatti Palle et al. 2004). The UV spectrometer used is an Acton VM-523-SG spectrometer at the Jet Propulsion Laboratory (JPL) ($\lambda/\Delta\lambda = 67{,}000$). The single channel detector used is a channel electron multiplier with a CsI coating, prepared by vacuum deposition at our laboratory. The holographic grating used with this spectrometer is a custom-coated B_4C concave 1200 grooves mm^{-1} grating with a horizontal (plane of dispersion) aperture ratio of f/28.8. The slow optical system results in a narrow field of view of the collision region of 3.8 mm (horizontal) by 2.4 mm (vertical). The UV photon

signal is detected by the spectrometer with an optic axis at 90° to the plane containing the crossed electron and HD target molecule beams. The interaction volume is approximately 2 mm^3. The polarization of the radiation is negligible for the HD transitions at 100 eV excitation energy. The magnetically collimated electron beam source is described in detail by Ajello et al. (1990). In brief, the thermionic electrons are created by heating a tungsten filament. The beam is collimated using an axially symmetric magnetic field of 100 G, which is generated by a solenoid system. The energy resolution of the electron beam is 1 eV. The absolute energy of the electron beam for energy scans is calibrated by measuring the appearance potential of the H, D Lyα from dissociative excitation of HD at 14.67 eV. We have performed wavelength scans at 100 eV with the HD target molecules formed by a capillary array effusing into the collision chamber. The optical path length is proportional to the distance from the collision region to the entrance slit (a distance of 11.05 cm). The low-pressure spectrum allowed nearly optically thin intensity measurements of all bands including the resonance bands (v', 0).

The measured spectra were corrected for relative inverse sensitivity of the spectrometer system consisting of the grating and channel electron multiplier. The relative inverse sensitivity calibration data was obtained by measuring the intensities of emissions from electron impact excitation of molecular hydrogen in the 800–1700 Å range and comparing them to the modeled H_2 intensities (Ajello et al. 1988; Liu et al. 1995). The resulting calibration data and fifth-degree polynomial fit for the HD experiment are shown in our recent paper for an SO_2 experiment (Vatti Palle et al. 2004).

The spectral resolution is 0.16 Å FWHM for the present experiment. The emission spectrum was obtained by scanning the grating from 900 to 1650 Å. The wavelength increment was 0.032 Å, which yielded a FWHM of five steps in the wavelength for the stepping motor. The integration time for each data point was 75 s in the far-ultraviolet (FUV) spectral region (1100–1650 Å) and 180 s in the extreme-ultraviolet (EUV) spectral region (900–1120 Å). The background HD gas pressure was 1.5×10^{-5} torr for the optically thin FUV region (without resonance bands) and 7.8×10^{-6} torr for the EUV region that includes all the resonance bands (800–1120 Å). The two spectra were smoothly joined in the 1100–1120 Å region by matching the intensities of rotational lines. The secondary absorption and emission processes were negligible. Line intensities below 900 Å were too weak at these integration times. Longer integration times were not possible at the prohibitively high cost of obtaining 99.9% purity of the HD. Nonuniform wavelength shifts of 0.1 Å can occur because of temperature fluctuations of the spectrometer housing (1 K) during the several day spectral scans of 10,000 channels in the EUV and 18,750 channels in the FUV.

3. THE ABSOLUTE CROSS SECTION OF H AND D Lyα AT 100 eV

The absolute cross section of the closely spaced D Lyα and H Lyα lines from electron impact dissociative excitation of HD at 100 eV was established by two techniques: the relative flow method and the static gas method. The relative flow calibration technique compares the relative intensities of the H, D Lyα and the H_2 Lyα (i.e., H Lyα from electron impact dissociative excitation of H_2) at a resolution of 0.8 Å FWHM in the cross-beam mode over a range of gas pressures. The UV photon signal varies linearly with the background gas pressure over the range 5×10^{-7} to 5×10^{-6} torr. At this spectral resolution the two Lyα peaks of HD (one due to H Lyα and the other due to D Lyα produced in dissociative excitation of the HD) are unresolved. The numerous rotational lines of Lyman and Werner appear as a continuum below the H, D Lyα feature. This continuum level furnishes the background value. At a higher resolution of 0.16 Å FWHM the H Lyα and the D Lyα peaks are measured to be of equal intensity. The ratio of the Lyα emission cross sections coming from HD (i.e., H, D Lyα) to those due to H_2 (i.e., H Lyα) was found to be 1.07.

Similarly, the cross section ratio in the static gas method (Ajello et al. 1990, 1991, 2003), in which the collision chamber is maintained at a uniform hydrogen gas pressure of 7×10^{-6} torr, was found to be 1.16. Thus, the two methods give nearly identical results within the experimental error. We find the average value of 1.115 for the two experimental methods for the ratio of the two Lyα cross sections. Using the cross section of the H Lyα from dissociative excitation of H_2 (Liu et al. 1998), we find the dissociative excitation cross section leading to emission of the H, D Lyα feature to be 7.98×10^{-18} cm^2 at 100 eV electron impact energy. The total emission cross section contribution from Lyman and Werner rotational lines laying between 1214.5 and 1216.5 Å is 2.0×10^{-19} cm^2. The principal remaining uncertainties to the cross section value are the signal statistics (1%), the systematic plus statistical difference of the two methods (8%), and pressure and electron beam current uncertainties (5%). Consequently, the cumulative error, 1 σ, in the absolute cross section of H, D Lyα is 14%. The uncertainty of the H, D Lyβ feature given later in this paper is estimated to be 25%.

4. THEORETICAL CALCULATIONS OF TRANSITION PROBABILITIES

We have calculated the emission transition probabilities between the B, B', C, and D upper rovibronic levels and the ground X rovibrational levels of HD, as well as the total emission lifetime of the upper states. The rovibrational levels within the electronic X ground state are obtained within the adiabatic approximation where the one-dimensional Schrödinger equation of the nuclear motion is solved, including the centrifugal barrier.

As already noted for H_2 by various authors (e.g., Abgrall et al. 2000; Senn et al. 1988), the upper electronic states may be coupled via rotational and radial coupling, and we obtain the rovibrational upper states by taking explicitly into account the nonadiabatic couplings and expanding the wave functions over the different Born-Oppenheimer (BO) wavefunction:

$$\Phi_{SvJ} = \sum_T \Psi_{TJ} f_{STvJ}. \quad (1)$$

Each Ψ_{TJ} is the product of the electronic BO wavefunction and the nuclear wavefunction describing the rotational motions. The nuclear wave function f_{STvJ} and the energy levels E_{vjJj} are obtained from the eigenfunctions and eigenvalues of the Schrödinger coupled equations whose diagonal terms are adiabatic potentials and off-diagonal terms are rotational and radial electronic coupling matrix elements. The formalism is described in detail by Senn et al. (1988).

The spontaneous emission transition probability (which is equivalent to the Einstein A-coefficient) between two discrete levels is given by the expression

$$A(v_j,\ v_i;\ J_j,\ J_i) = \frac{4}{3\hbar^4 c^3 (2J_j + 1)} (E_{vjJj} - E_{viJi})^3 |M_{S\alpha}|^2, \quad (2)$$

where E_{vJ} is the energy of the level (v, J), $M_{S\alpha}$ is the electric dipole matrix element between wavefunctions of excited $S(v_J,\ J_J)$ and ground electronic $X(v_i,\ J_i)$ states, and α indicates whether the spectroscopic branch label is P, Q, or R.

When the emission takes place into the X continuum states, the expression has to be modified to take into account the different normalization of the continuum wave functions. Then

$$A(v_j,\ e_i;\ J_j,\ J_i) = \frac{4}{3\hbar^4 c^3 (2J_j + 1)} (E_{v_j J_j} - E_{e_i J_i})^3 |M_{S\alpha}|^2, \quad (3)$$

where the kinetic energy of dissociating atoms e_i replaces the vibrational indices v_i and the continuum wave functions satisfy the normalization relative to energy.

The total emission probability, which is the inverse of the radiative lifetime, includes a sum over all possible emission processes:

$$A_t(v_j;\ J_j) = A_c(v_j;\ J_j) + \sum_{v_i, J_i} A(v_j,\ v_i;\ J_j,\ J_i), \quad (4)$$

where $A_c(v_j;\ J_j)$ is the total emission probability toward the continuum, which is given by

$$A_c(v_j;\ J_j) = \sum_{J_i} \int_0^\infty A(v_j,\ e_i;\ J_j,\ J_i)\, de_i, \quad (5)$$

where the selection rules on J are taken into account and where an integral is performed over the kinetic energy of the continuum level.

The dipole matrix elements, $M_{S\alpha}$, appearing in equation (3) are given by the following expressions:

$$\begin{aligned}
M_{SP} &= (J_i + 1)^{1/2} \left\{ \left\langle f_{B v_j J_j} | M_{BX} | f_{X v_i J_i} \right\rangle + \left\langle f_{B' v_j J_j} | M_{B'X} | f_{X v_i J_i} \right\rangle \right\} \\
&\quad + (J_i)^{1/2} \left\{ \left\langle f_{C^+ v_j J_j} | M_{CX} | f_{X v_i J_i} \right\rangle + \left\langle f_{D^+ v_j J_j} | M_{DX} | f_{X v_i J_i} \right\rangle \right\}, \\
M_{SQ} &= (2J_i + 1)^{1/2} \left\{ \left\langle f_{C^- v_j J_j} | M_{CX} | f_{X v_i J_i} \right\rangle + \left\langle f_{D^- v_j J_j} | M_{DX} | f_{X v_i J_i} \right\rangle \right\}, \\
M_{SR} &= (J_i)^{1/2} \left\{ \left\langle f_{B v_j J_j} | M_{BX} | f_{X v_i J_i} \right\rangle + \left\langle f_{B' v_j J_j} | M_{B'X} | f_{X v_i J_i} \right\rangle \right\} \\
&\quad - (J_i + 1)^{1/2} \left\{ \left\langle f_{C^+ v_j J_j} | M_{CX} | f_{X v_i J_i} \right\rangle + \left\langle f_{D^+ v_j J_j} | M_{DX} | f_{X v_i J_i} \right\rangle \right\},
\end{aligned}$$

where M_{BX}, M_{CX}, $M_{B'X}$, and M_{DX} are the real values of electronic transition moments, which are functions of the internuclear distance and calculated in the BO approximation.

Since HD is not a homonuclear molecule, the center of mass does not coincide any more with the center of charge. Therefore, in the case of HD, gerade and ungerade labels do not define exact good quantum numbers for the rovibronic states, and a weak rovibrational coupling can take place between u and g BO states. This is demonstrated by the experimental observation of weak dipole transitions between the g-g (such as EF–X, GK–X, etc.) electronic states (see, e.g., Dabrowski & Herzberg 1976 and Hinnen et al. 1995). This weak effect appears especially in the case of accidental coincidence between u and g uncoupled rovibrational states, and we did not include it for generating our emission transition probability calculations in the present paper.

4.1. *Electronic Matrix Elements*

In Abgrall et al. (2000), we had smoothed the small inaccuracies of the ab initio matrix elements and the effect of the limited expansion by a small empirical adjustment. This has not been done here, because there are not enough accurate experimental levels. Moreover, the local $g-u$ couplings shift levels in a random way.

The calculations were performed by introducing the most recent and accurate matrix elements values. The diagonal matrix elements (BO potentials and adiabatic corrections) of the B and B' states as well as the $B-X$ and $B'-X$ electronic transition matrix elements are taken from Staszewska & Wolniewicz (2002) and Wolniewicz & Staszewska (2003a) and those for the C and D states are taken from Wolniewicz & Staszewska (2003b). The off-diagonal rotational and radial matrix elements are taken from Wolniewicz & Dressler (1988).

The adiabatic potential for the ground electronic X state is taken from Wolniewicz (1993). The transition wavenumbers have been obtained by using the experimental terms for the lower states. Then the comparison with the available experimental measurements reflects the accuracy of our calculated upper states. We find that, when comparison is available, our calculated values are generally within 2 cm^{-1} of the experimental values of Dabrowski & Herzberg (1976). This comparison confirms that the g-u coupling borrowing effect, which reduces the allowed g-u emission probability of u-state and transfers the difference to forbidden g-g emission probability of a close g-state, is generally weak.

5. THE SPECTRAL MODEL

The prime goal of the laboratory program is to determine the emission cross sections of the $n = 2$ and 3 Rydberg states (B, B', C, and D) of HD at 100 eV and to verify the accuracy of the theoretical calculations presented in § 4. The model used to estimate the cross sections from the laboratory spectrum has been described in previous papers on H_2 (Liu et al. 1995, 1998, 2000, 2002, 2003; Jonin et al. 2000). We will describe it in a general way here. The model calculates the intensity of UV discrete and continuum transitions in an HD gas excited by electrons (E_e = 100 eV), using transition probabilities based upon the rotational-vibrational-electronic wavefunctions of the ground and excited states from the previous section. The population of the ground state rotational levels is controlled by the gas temperature. The $J'' = 1$ level contains the largest rotational population, roughly 40% of the population at 300 K. The $Q1$ lines of the $np\pi$ Rydberg series are the most strongly self-absorbed rotational lines. The ground state molecules in vibrational and rotational thermal equilibrium are excited into the various rovibronic states according to the volumetric excitation rate $g(\alpha, \nu, J, E_e)$. The photoemission intensity into the various branches from rovibronic state $|\langle \alpha, \nu, J \rangle|$ is partitioned according to the emission branching ratio and predissociation yield, $\eta_P(\alpha, \nu, J)$ (Liu et al. 2000). The volumetric photoemission rate, I, including self-absorption is given by

$$\begin{aligned}
I(X,\ a,\ v_f,\ v,\ J_f,\ J) &= \frac{A(X, a,\ v_f,\ v,\ J_f,\ J)}{A(X,\ a,\ v,\ J)} g(a,\ v,\ J,\ E_e) \\
&\quad \times [1 - \eta_P(a,\ v,\ J)] \mathrm{Tr}(X,\ a,\ v,\ J,\ T),
\end{aligned} \quad (6)$$

where $A(X,\ \alpha,\ v,\ J) = \sum_{v_f, J_f} A(X,\ \alpha,\ v_f,\ v,\ J_f,\ J)$ and $A(X,\ \alpha,\ v_f,\ v,\ J_f,\ J)$ is the Einstein A-coefficient for spontaneous transition from the excited state $|\langle \alpha, \nu, J \rangle|$ to the state $|\langle X, \nu_f, J_f \rangle|$ of the $X\,^1\Sigma_g^+$ ground state and $A(X,\ \alpha,\ v,\ J)$ is the total emission probability (Liu et al. 1995, 1998; Jonin et al. 2000). $\mathrm{Tr}(X,\ \alpha,\ v,\ J,\ T)$ is the transmission function for self-absorption through HD gas at temperature, T (Ajello et al. 1998, 2001). Deviations from the single-scattering in the determination of experimental

emission cross sections are negligible. The excitation rate $g(\alpha,\ \nu,\ J,\ E_e)$ is proportional to the mean cross section in the $v'' = 0, J''$ initial level, the population density in level J'' of the ground state, and the electron flux. Equation (7) shows that the mean cross section is the weighted average of the population in the J'' rotational level for each branch, the excitation cross section for the branch, and the impact electron flux F_e at energy E_e (Liu et al. 1998). The volumetric excitation rate is given by

$$g(a,\ v,\ J,\ E_e) = F_e \sum_i N_i Q_{ij}(E_e). \quad (7)$$

The quantity $Q_{ij}(E_e)$ is the excitation cross section at 100 eV and is calculated from a known transition probability, assuming the validity of the Born approximation. The subscripts (ij) represent the collection of quantum numbers (α, ν_f, J_f) and (X, ν, J) of the ground and excited states (Liu et al. 1995, 2000). For negligible self-absorption the photoemission intensity in equation (7) is proportional to the mean emission cross section. In the present work we used the total transition probabilities of the previous section for the B, B', C, and D, that is, the $n = 2$ and 3 members of the Rydberg $np\pi$ and $np\sigma$ series.

The model spectra at 160 mÅ FWHM for each of the B, B', C, and $D \rightarrow X$ transitions are shown in Figure 1 without self-absorption, cascading, and (pre)dissociation at an electron impact energy of 100 eV. The synthetic model spectra cover the range from 800 to 1700 Å. The wavelength region of interest of the present experimental study comprises a slightly narrower region from 900 to 1700 Å, which is a spectral region that contains all the emission from the Rydberg $n = 2$ states and most of the emissions from the $n = 3$ states. Approximately 25% of the B' and D band systems lie below 900 Å. This model must be used to account for the missing rotational lines for wavelengths below 900 Å in order to estimate the total UV emission from HD. It is clear that the Werner band emissions dominate the emission spectrum in the wavelength region from 950 to 1200 Å, whereas Lyman band transitions dominate the emission from 1200 to 1650 Å. The strongest part of the Lyman continuum lies in the wavelength range between 1500 and 1600 Å. The model omits the unknown contribution from the $n = 4$ Rydberg level comprising the $B''-X$ and $D'-X$ band systems. A comparable analysis of H_2 for the same bands has shown that $n = 4$ makes a small contribution to the emission spectrum in the 900–950 Å region. The unmeasured 750–900 Å region would be dominated by the $n = 4$ Rydberg bands. The set of strongest Werner rotational lines are all $Q1$ branch lines. The strongest line is the $Q1(1, 4)$ rotational line at 1139.74 Å, followed by several other nonresonant Q-branch rotational lines at 1191.18 Å $Q1(2, 6)$ and 1202.36 Å $Q1(3, 7)$, and a resonant band at 969.81 Å $Q1(2, 0)$. There are also very strong $R0$ lines for these same vibrational transitions also originating from $J' = 1$.

There are two important ways for producing the strong vibrational transition progressions for the Lyman band system. In the first, called direct mode, the electrons induce a g-u dipole allowed transition toward the rovibrational levels of B (especially $v' = 6$–12), then the excited HD returns to rovibrational level of X by emitting UV radiation. In the second, called cascade mode, the electrons induce a dipole-forbidden transition principally toward gerade symmetry upper intermediary electronic states, like $EF\ ^1\Sigma_g^+$, $GK\ ^1\Sigma_g^+$, and $H\bar{H}\ ^1\Sigma_g^+$, amid which the most important is by far EF, next the intermediary rovibrational states emit allowed infrared radiations toward $B\ ^1\Sigma_u^+$ states (especially $v' = 0$–2), finally the rovibrational states emit UV radiation toward the $X\ ^1\Sigma_g^+$ state. The rigorous $g \leftrightarrow u$ rule for the dipole

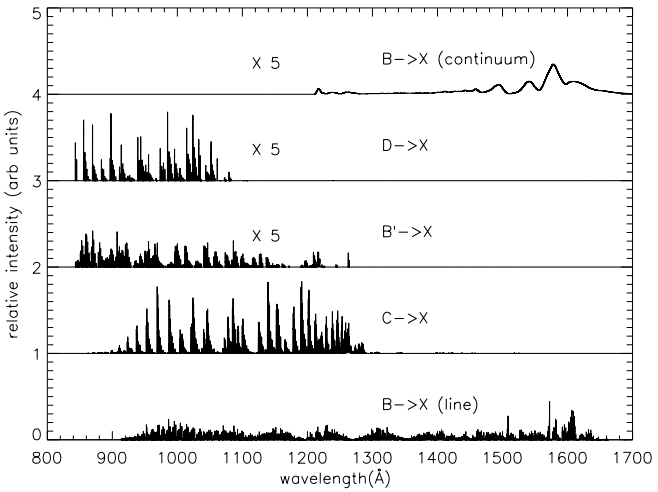

FIG. 1.—Model electron-induced fluorescence spectrum of the $B\ ^1\Sigma_u^+ \rightarrow X\ ^1\Sigma_g^+$ (discrete), $C\ ^1\Pi_u \rightarrow X\ ^1\Sigma_g^+$, $B'\ ^1\Sigma_u^+ \rightarrow X\ ^1\Sigma_g^+$, $D\ ^1\Pi_u \rightarrow X\ ^1\Sigma_g^+$, and $B\ ^1\Sigma_u^+ \rightarrow X\ ^1\Sigma_g^+$ (continuum) band systems for the HD molecule. The intensities of the $B'\ ^1\Sigma_u^+ \rightarrow X\ ^1\Sigma_g^+$, $D\ ^1\Pi_u \rightarrow X\ ^1\Sigma_g^+$, and $B\ ^1\Sigma_u^+ \rightarrow X\ ^1\Sigma_g^+$ (continuum) band systems have been expanded by a factor of 5.

radiation is no longer strictly obeyed in the HD due to the small breakdown of the BO approximation in a rotating molecule (Dabrowski & Herzberg 1976). The first excited $^1\Sigma_g^+$ state of the hydrogen molecule and its isotopes is a double minimum resulting from an avoided crossing and the two minima are referred to as the $EF\ ^1\Sigma_g^+$ state (Kolos & Wolniewicz 1969). We call the EF–B cascade band the Lyman band produced via the cascade mechanism with EF as intermediary g electronic state. Our theoretical model takes into account only the first mechanism. However, the experimental data will show the importance of the cascade mode. The strongest direct excitation rotational lines are at 1508.53 Å $P1$, $P2$, $P3$, $P4$, $R0$, $R1$, $R2$, and $R3$ (12, 16) and 1572.40 Å $P1$, $P2$, $P3$, $P4$, $R0$, $R1$, $R2$, and $R3$ (9, 16).

The strongest $D-X$ features are found at 984.41 and 1023.86 Å. These features are a blend, respectively, of $Q1$, 2 and $R0$, 1 (1, 4) and (2, 6) rotational lines. Only the feature at 984.41 Å is fully resolved in the experimental spectrum at 0.16 Å FWHM, but it appears very weak on a relative basis compared to the Lyman and Werner bands. For this reason the $n = 4$ members of the two Rydberg series, which are the upper principal quantum numbers for the $B''-X$ and $D'-X$ bands, are not expected to contribute strongly to the regression analysis of the next section. In the spectral region below 900 Å lie the two strong $D-X$ features at 855.79 and 897.87 Å, which are also a blend, respectively, of $Q1$, 2 and $R0$, 1 (3, 0) and (1, 1) rotational lines.

6. ANALYSIS OF THE HIGH-RESOLUTION LABORATORY SPECTRUM

We have analyzed the laboratory high-resolution spectrum observations with the model given in the previous section. We compare the data and modeled synthetic spectrum using a regression analysis best-fit approach, a method similar to that presented in Ajello et al. (1998, 2001, 2005) for the analysis of the UV observations of the Jupiter aurora. The first vector (a linear array of 25,000) in the regression involves the sum of the Lyman and Werner discrete and continuum emissions. We assess this summed intensity as a constraint to the regression analysis. The constraint is based upon our theoretical calculation of the oscillator strengths for the Lyman and Werner band systems and the Modified Born approximation study of the excitation cross

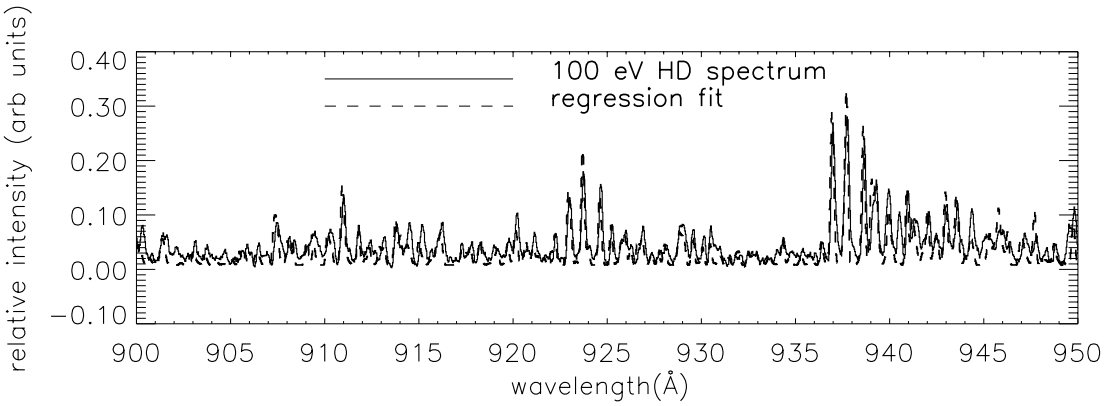

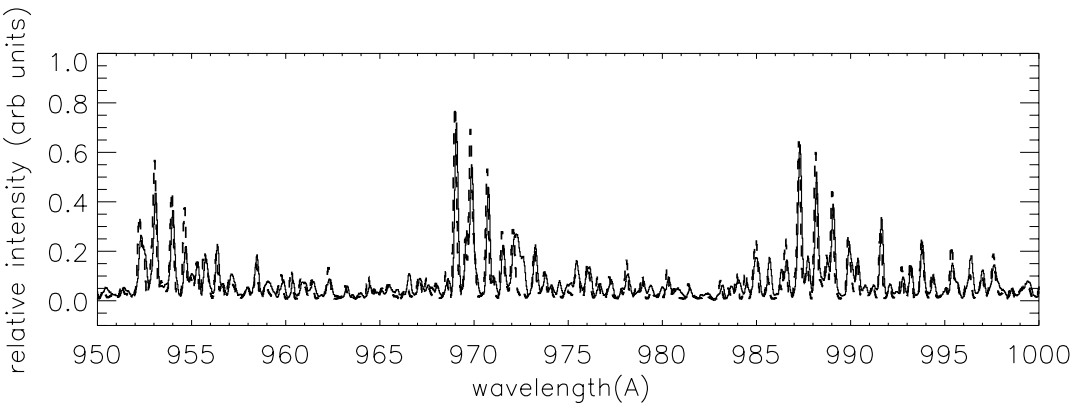

FIG. 2*a*

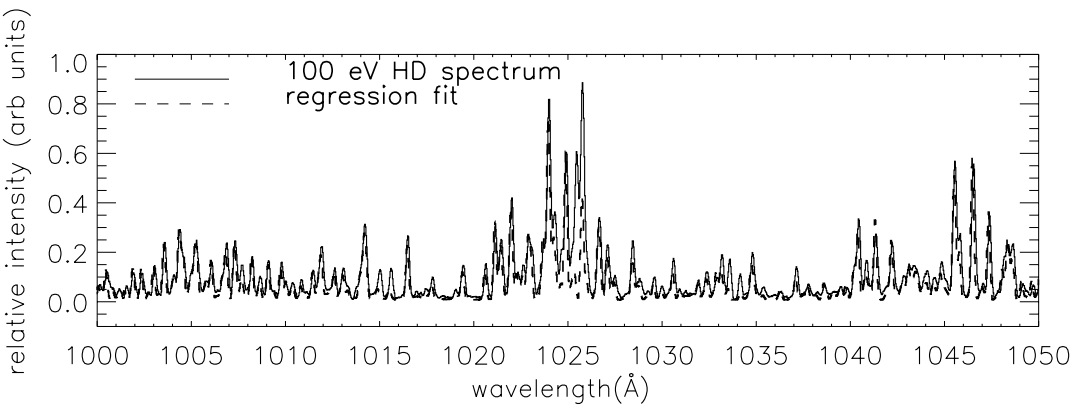

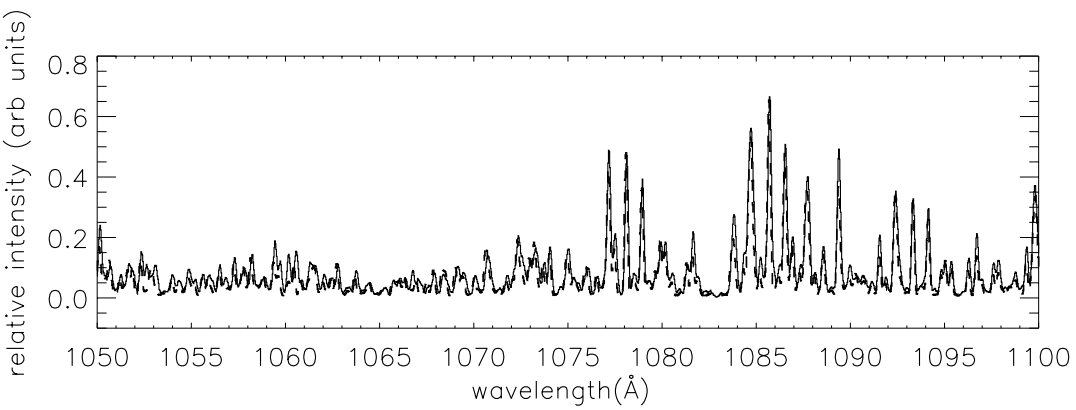

FIG. 2*b*

FIG. 2.—Comparison between the experimental spectrum (*solid lines*) and a model synthetic spectrum (*dashed lines*) based on the regression analysis obtained at 300 K gas temperature, 100 eV electron impact energy, and 0.160 Å FWHM from 900 to 1650 Å. The experimental spectrum has been corrected for the instrumental sensitivity variation as described in Vatti Palle et al. (2004). The model spectrum is based on the line intensities, calculated using the transition probabilities of this paper, convoluted with the triangular instrument slit transfer function: (*a*) 900–1000 Å, (*b*) 1000–1100 Å, (*c*) 1100–1200 Å, (*d*) 1200–1300 Å, (*e*) 1300–1400 Å, (*f*) 1400–1500 Å, (*g*) 1500–1600 Å, and (*h*) 1600–1650 Å.

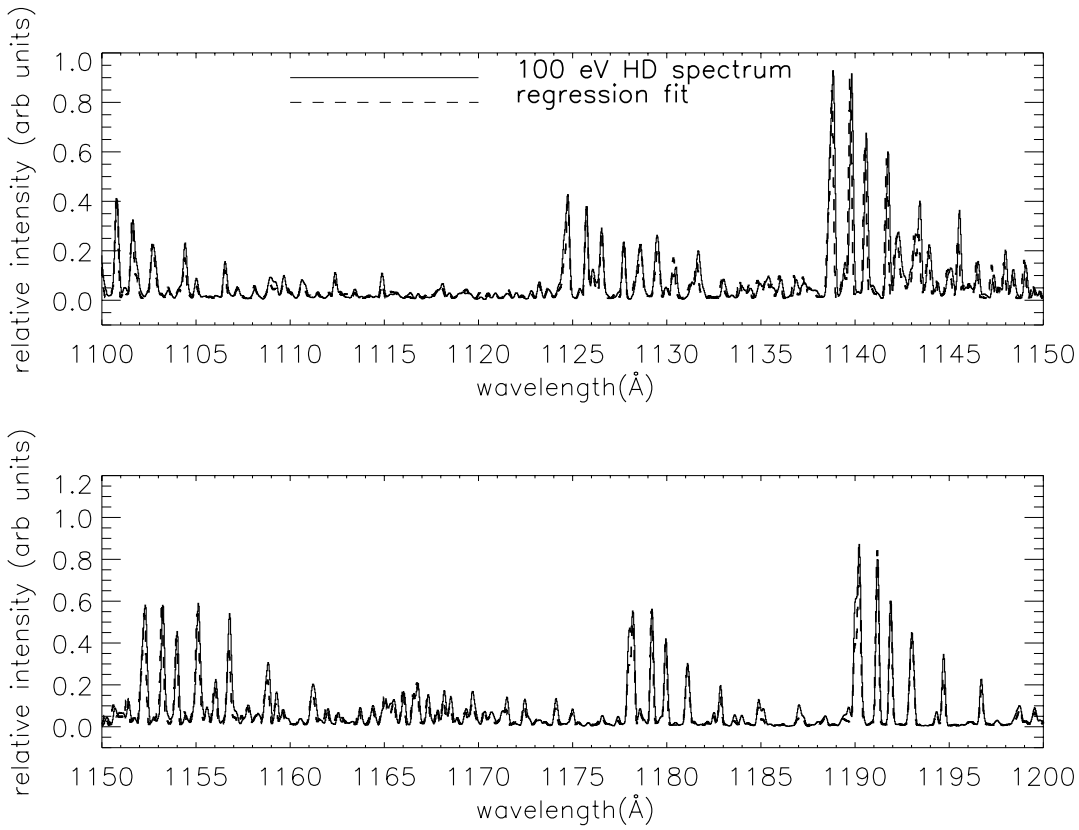
100 eV HD spectrum
regression fit
relative intensity (arb units)
wavelength(Å)
1.0
0.8
0.6
0.4
0.2
0.0
1100 1105 1110 1115 1120 1125 1130 1135 1140 1145 1150
1.2
1.0
0.8
0.6
0.4
0.2
0.0
1150 1155 1160 1165 1170 1175 1180 1185 1190 1195 1200

FIG. 2*c*

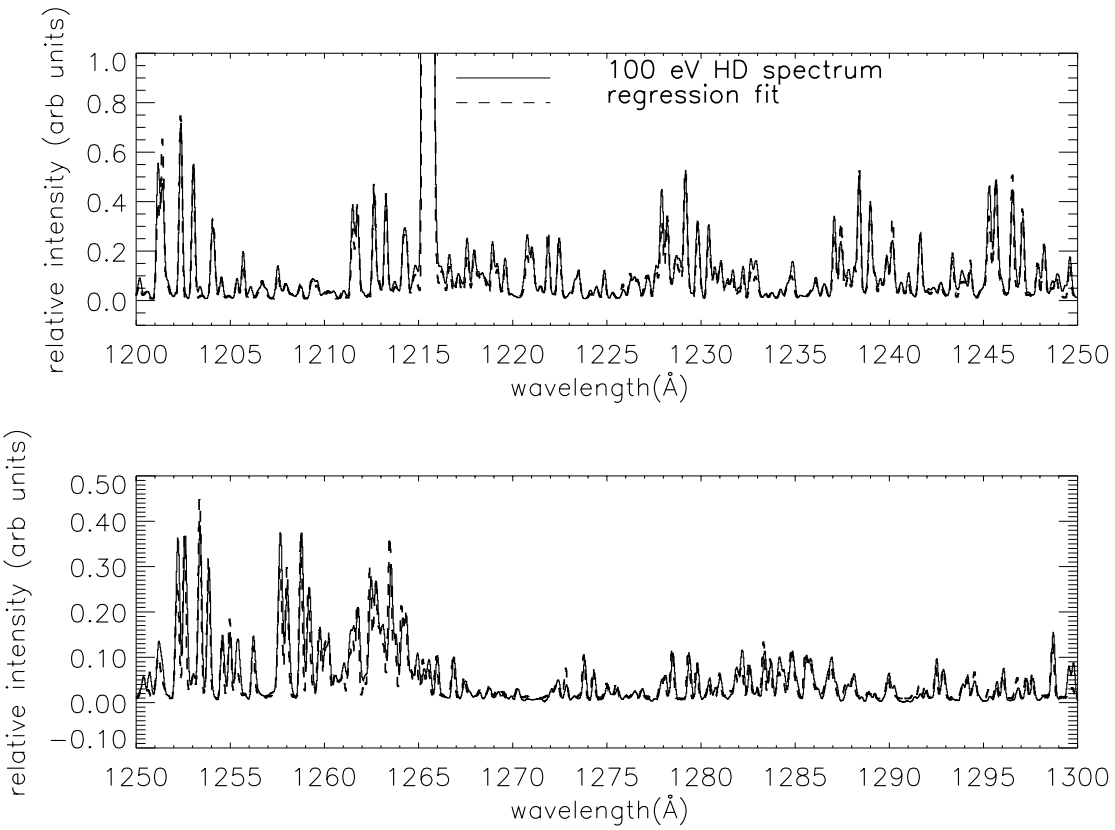
100 eV HD spectrum
regression fit
relative intensity (arb units)
wavelength(Å)
1.0
0.8
0.6
0.4
0.2
0.0
1200 1205 1210 1215 1220 1225 1230 1235 1240 1245 1250
0.50
0.40
0.30
0.20
0.10
0.00
−0.10
1250 1255 1260 1265 1270 1275 1280 1285 1290 1295 1300

FIG. 2*d*

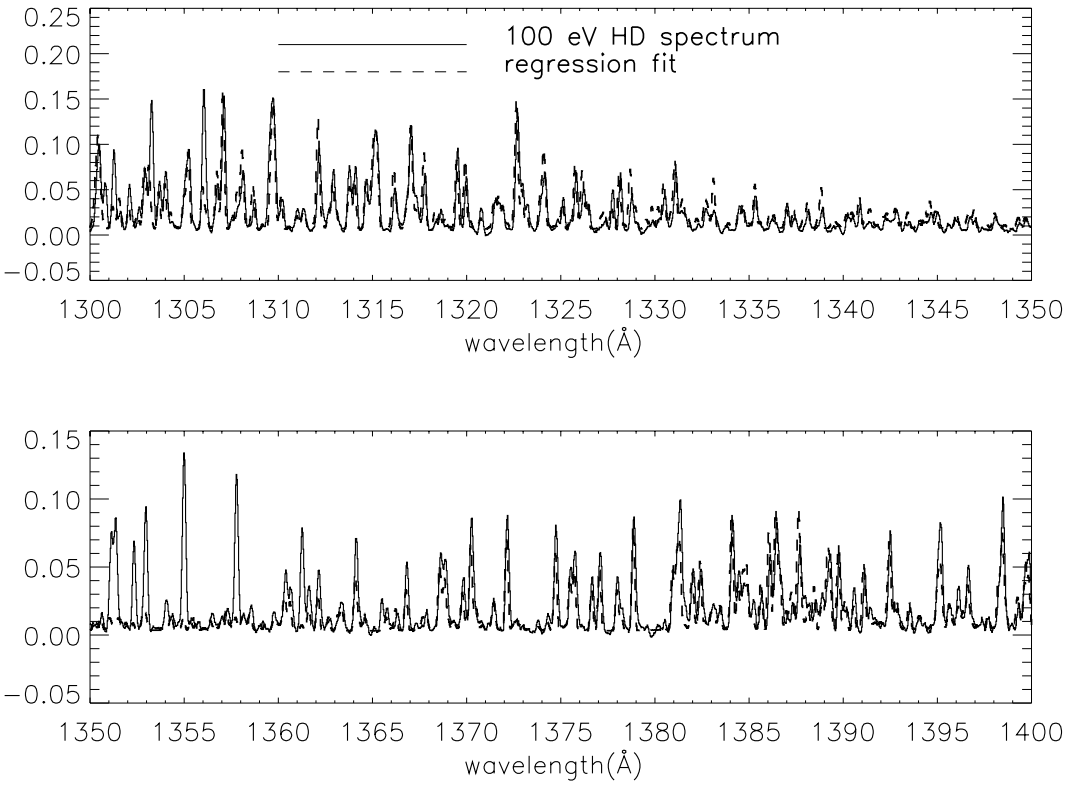
100 eV HD spectrum
regression fit
0.25
0.20
0.15
0.10
0.05
0.00
−0.05
1300 1305 1310 1315 1320 1325 1330 1335 1340 1345 1350
wavelength(Å)
0.15
0.10
0.05
0.00
−0.05
1350 1355 1360 1365 1370 1375 1380 1385 1390 1395 1400
wavelength(Å)

FIG. 2*e*

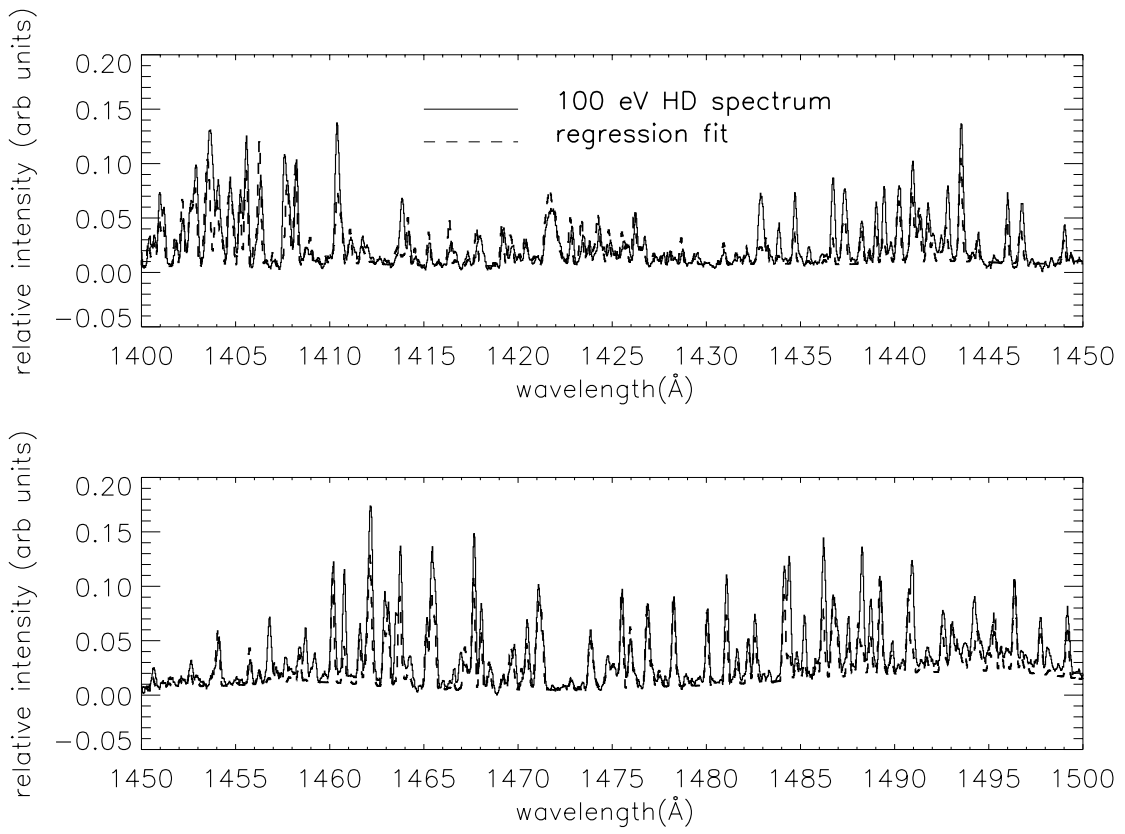
relative intensity (arb units)
100 eV HD spectrum
regression fit
0.20
0.15
0.10
0.05
0.00
−0.05
1400 1405 1410 1415 1420 1425 1430 1435 1440 1445 1450
wavelength(Å)
relative intensity (arb units)
0.20
0.15
0.10
0.05
0.00
−0.05
1450 1455 1460 1465 1470 1475 1480 1485 1490 1495 1500
wavelength(Å)

FIG. 2*f*

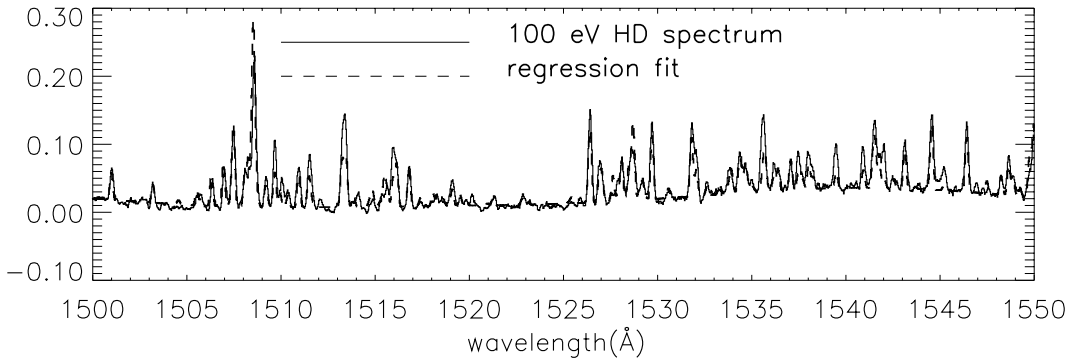

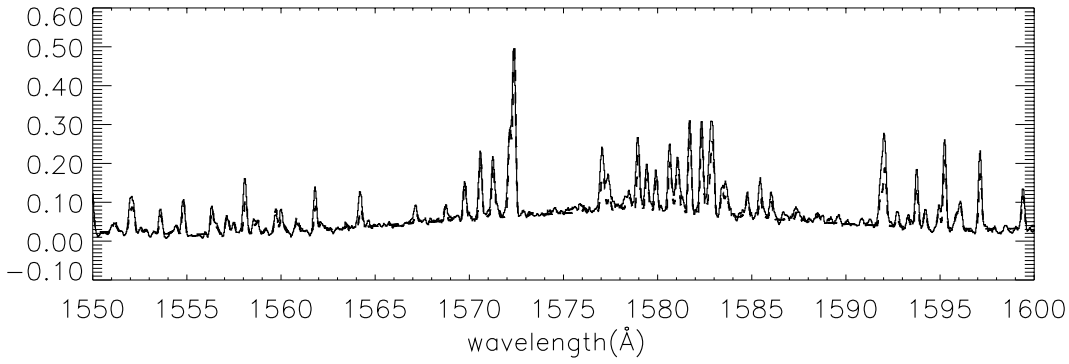

FIG. 2*g*

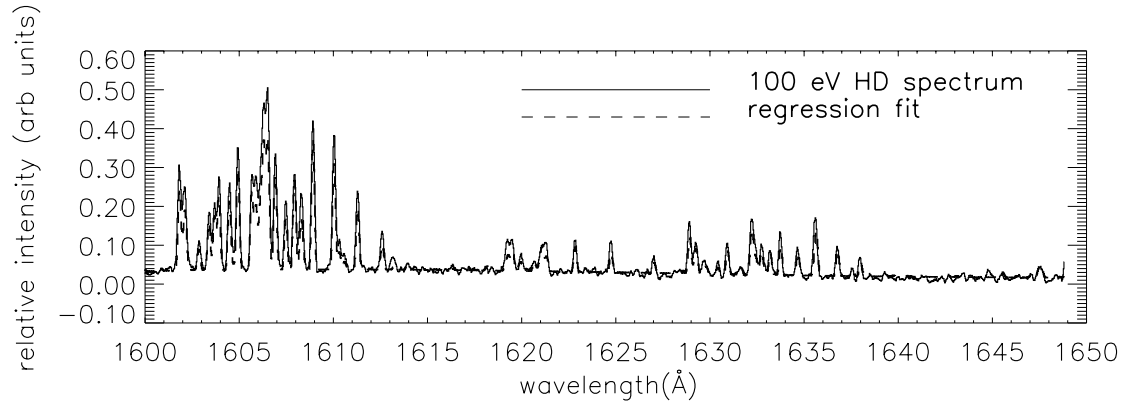

FIG. 2*h*

sections of the Lyman and Werner bands of H_2 (Liu et al. 1998). From the HD Lyman band oscillator strengths, we calculate that the Lyman continuum contributes 29.7% of the summed intensity of the discrete rotational lines and continuum of the Lyman band system. We have explained the calculation of continuum dissociation yields previously for H_2 (Abgrall et al. 1997) and D_2 (Abgrall et al. 1999). The Modified Born approximation, which is an analytic expression for the excitation cross section as a function of energy, can be used to relate the relative intensities of the Lyman and Werner bands for electron impact-induced fluorescence at 100 eV. For the constraint, we make the assumption that the shapes of the Lyman and Werner excitation functions for HD and H_2 are the same. We can calculate the direct excitation cross sections for the Lyman and Werner cross sections at 100 eV. Using the oscillator strengths of HD we find that the excitation cross sections at 300 K and 100 eV of the $B\ ^1\Sigma_u^+$ and $C\ ^1\Pi_u$ states are 2.57×10^{-17} and 2.54×10^{-17} cm^2, respectively.

There are three remaining independent spectral vectors in the regression analysis. The next two vectors consist of the discrete excitation transitions of the two $n = 3$ HD Rydberg bands (B'–X and D–X). The fourth vector is the H, D Lyα lines, a single vector centered at the mean value of the H Lyα at 1215.67 Å and the D Lyα at 1215.34 Å. The omission of the *EF*, *GK*, and $H\bar{H} \rightarrow B$ cascade model vector may lead to a serious underestimation of the intensity values in the FUV spectral region where the $v' = 0, 1$ cascade progressions of the gerade states are strongly excited. We will show that cascade is very important in the 1300–1600 Å wavelength region. We will make a calculation of the *EF*-*B* oscillator strengths needed to estimate the major cascading contribution to the Lyman band system in § 8.

Based on the regression analysis, we show in Figure 2 the best fit of the synthetic spectrum model to the laboratory spectrum obtained in the 900–1650 Å region. The figure is divided into eight subfigures, 2*a*, 2*b*, 2*c*, 2*d*, 2*e*, 2*f*, 2*g*, and 2*h*, of 100 Å each. The absolute emission cross sections of the $n = 2$, 3 Rydberg

series members along with the H, D Lyα cross sections and estimates for cascade cross sections in the FUV and the sum of cascade and $n > 3$ Rydberg series members in the EUV at 100 eV are given in Table 1. The $n = 3$ Rydberg series emission cross sections ($B'-X$ and $D-X$) are calculated from the regression model coefficients of $n = 3$ compared to regression model coefficients of the $n = 2$ Rydberg series members. In Table 1 the emission cross section for the Lyman bands is the sum of the direct excitation cross section to $B\ ^1\Sigma_u^+$ and the cascade cross section to $B\ ^1\Sigma_u^+$ from the overlying gerade rovibrational transitions. For the other band systems cascading is negligible. Based on the regression model, the individual emission cross sections include contributions for direct excitation to the B, B', C, and D states and the cascading from the gerade states, the latter as explained below, from the extended UV wavelength region comprising all rotational lines and continua from 800 to 1700 Å.

The most important omission to the HD Rydberg model band system is the neglect of possible cascades coming from the gerade excited electronic states, particularly $EF\ ^1\Sigma_g^+ - B\ ^1\Sigma_u^+ - X\ ^1\Sigma_g^+$. The bands produced by these cascades are found throughout the UV region at wavelengths greater than 900 Å. By using the arguments from our understanding of the cross sections of the H_2 molecule, we expect about 70%–80% of the B-state cascade bands to be located above the H Lyα wavelength (1216 Å). Below the H Lyα wavelength, approximately 10% of the cascade bands arise from the EF, GK, and $H\bar{H}\ ^1\Sigma_g^+ \rightarrow C\ ^1\Pi_u$ cascade transitions (Liu et al. 2002). The remaining 10%–20% of the cascade cross sections for wavelengths below H Lyα is distributed among the other Rydberg band systems, including most strongly the Lyman bands. The cascade contributions from the B' and D states amount to less than 1% of the total HD cascade cross section. We show in Table 1 the estimate of the B (cascade) cross section to be 3.20×10^{-18} cm^2 (for wavelengths above the H Lyα), based upon the discrepancy in intensity between the measured signal in the FUV and the best-fit direct excitation FUV model in Figure 2. The $B\ ^1\Sigma_u^+$ emission cross section is found to be 2.89×10^{-17} cm^2. As a lower limit, the cascade cross section contributes 11% of the emission cross section at 100 eV.

The other Rydberg emission cross sections of the other Rydberg states are found to be 2.54×10^{-17} cm^2 for $C\ ^1\Pi_u \rightarrow X\ ^1\Sigma_g^+$, 1.7×10^{-18} cm^2 for $D\ ^1\Pi_u \rightarrow X\ ^1\Sigma_g^+$, and 2.2×10^{-18} cm^2 for $B'\ ^1\Sigma_u^+ \rightarrow X^1\Sigma_g^+$. We also give in Table 1 the first estimate of the H, D Lyβ cross section to be 4.0×10^{-19} cm^2 at 100 eV.

Besides molecular band radiative emission, direct dissociation or predissociation of the molecule with formation of an excited atom is another way for de-excitation after electron impact. We can see in Jonin et al. (2000) that dissociation is negligible for B and C states but that for B' and D states the dissociative yields are 54% and 32%, respectively. We expect the same behavior for HD.

The $3p\pi\ D\ ^1\Pi_u^+$ state is strongly predissociated by the continuum of the B' state for $v' > 3$. Above the $v' = 3$ level, the emission yield becomes zero. Strong absorption features of the $D\ ^1\Pi_u^+$ state to the $v' = 17$ have been observed by Dehmer & Chupka (1983) and are denoted by the broadened line widths. On the other hand, the $3p\pi\ D\ ^1\Pi_u^-$ state can decay by modes, emission or predissociation. Unlike in the case of H_2, the $D\ ^1\Pi_u^-$ state in HD can interact with another state of $^1\Pi^-$ symmetry (the most likely state is $I\ ^1\Pi_g^-$ state according to Dehmer & Chupka 1983) to cause the observed complete predissociation above the dissociation limit. Thus, predissociation is very strong for both: the $3p\pi\ D\ ^1\Pi_u^-$ state and the $3p\pi\ D\ ^1\Pi_u^+$ state. Then it is expected that radiation yields are lower for HD than for H_2 or D_2.

TABLE 1

Estimated Band System Cross Sections of HD at 100 eV

Band System	Cross Section (10^{-17} cm^2) HD	H_2	D_2
$B\ ^1\Sigma_u^+$ (discrete)	1.81	1.90[a]	1.76[b]
$B\ ^1\Sigma_u^+$ (continuum)	0.76	0.72[a,c]	0.70[b]
$B\ ^1\Sigma_u^+$ (direct)	2.57	2.62[a]	2.50[b]
$B\ ^1\Sigma_u^+$ (cascade)	0.32[d]	0.50[e]	
$B\ ^1\Sigma_u^+$ (emission)	2.89[d]	3.12	
$C\ ^1\Pi_u$	2.54	2.40[a]	2.46[b]
$B'\ ^1\Sigma_u^+$	0.22	0.21[a]	
$D\ ^1\Pi_u$	0.17	0.28[a]	
H Lyβ	0.04	0.03[f]	
Other direct bands (B'', D'), B (cascade) and H Lyγ, δ, ..., from 800 to 1200 Å	~0.7		

[a] Jonin et al. (2000); Liu et al. (1998).
[b] Abgrall et al. (1999).
[c] Abgrall et al. (1997).
[d] Lower limit since cascade was only measured for wavelengths above 1216 Å.
[e] Dziczek et al. (2000).
[f] Ajello et al. (1996).

We list in Table 1 the set of Lyman and Werner 100 eV excitation and emission cross sections for the hydrogenic isotopes: HD, H_2, and D_2, which were measured in our laboratory over the past 10 years. The cross section values are the same to within about 6%. The electronic structures of the three species are nearly identical, which is the major effect in determining the electronic cross section.

The strongest rotational lines for the $B\ ^1\Sigma_u^+ \rightarrow X\ ^1\Sigma_g^+$ Lyman system from cascade are found in the $(v' = 0, v'')$ vibrational progression. In Figure 2 the $P1$, $P2$, $P3$, and $R0$, 1 (0, 4) rotational lines near 1306 Å and $P1$, $P2$, $P3$, and $R0$, 1 (0, 5) rotational lines near 1358 Å are shown to be particularly strong. The same progression values for H_2 were shown to dominate its cascade spectrum (Dziczek et al. 2000; Liu et al. 2002).

7. H, D Lyα EXCITATION FUNCTION

We have measured the excitation function for the H, D Lyα production in electron impact dissociation excitation of HD from threshold to 800 eV. The excitation function was put on an absolute scale by normalizing it to the dissociative excitation emission cross section of 7.98×10^{-18} cm^2 at 100 eV. The dissociative excitation cross section for H, D Lyα at 100 eV is determined by comparing the Lyα relative intensity in HD gas to that in H_2 gas in both a gas swarm and a gas jet cross beam environment (Liu et al. 1998). The laboratory-measured dissociative excitation cross section for production of the H, D Lyα are analytically represented, within experimental error, using the semiempirical relation (Jackman et al. 1977; Bhardwaj & Michael 1999a; Vatti Palle et al. 2004)

$$\sigma(E) = \frac{q_0 F}{W^2}\left[1 - \left(\frac{W}{E}\right)^{\alpha}\right]^{\beta}\left(\frac{W}{E}\right)^{\Omega}. \quad (8)$$

Here $q_0 = 4\pi a_0^2 R^2$ and has the numerical value 6.513×10^{-14} eV^2 cm^2, E is the energy of incident electron in eV, W is the "fitting" threshold energy for the process in eV, while $W_{\rm th}$ is the "real" threshold of the process in eV (cf. Table 2), and α, β, Ω, and

TABLE 2
Model Fit Parameters for H, D Lyα Cross Sections

Parameter	Process		
	I	II	III
W (eV)	14.67	23.0	30.2
α	0.7	1.5	1.5
β	1.15	1.7	2.7
Ω	1.7	0.78	0.75
F	0.212	0.053	0.26
W_{th} (eV)	14.67	23.0	30.2

F are the fitting parameters. The model-fitted and laboratory-measured cross sections are shown in Figure 3 and the model parameters are given in Table 2. The inset in Figure 3 shows the model fit in the lower energy region (energy in logarithmic scale): the region that is difficult to view in the full plot in linear scale. The inset of Figure 3 also helps describe the shape of the Lyα excitation function in the near threshold and low-energy regions. The agreement between the model and data is fairly good keeping in view of the scatter in experimentally measured excitation function data. The advantage of representing the cross sections analytically is the great ease in using cross section values in comprehensive theoretical models, and their usage removes any ambiguity about the actual cross sections used in model calculations (e.g., Bhardwaj & Michael 1999a, 1999b; Bhardwaj 1999, 2003).

There are several singlets (singly and doubly excited) and triplet states that contribute to the excitation function of the H, D Lyα (e.g., Ajello et al. 1991, 1995a, 1995b). As can be observed from Table 2, the excitation function has been modeled using three different processes, having thresholds at 14.67 eV (process I), 23.0 eV (process II), and 30.2 eV (process (III). We have taken these three thresholds as identified by Ajello et al. (1995b) for the production of the H Lyα emission from dissociative excitation of H_2. These processes can adequately represent the cross section shape and magnitude of the H, D Lyα line (cf. Fig. 3). The cross section $\sigma(E)$ in equation (8) is the sum of contributions from the three independent processes I, II, and III. The H, D Lyα cross section peaks at $\sim$70 eV with a value of 8.6×10^{-18} cm^2. The maximum contribution at energies higher than the cross section peak comes from the singlet states (process III), which peaks at 100 eV, and it also provides the shape of a modified Born approximation to the excitation function at high energies. The sharp rise in the excitation function near threshold is apparently produced by a combination of exchange and resonance cross sections of triplet and singlet states. The excitation function in this region is fitted with process I having threshold at 14.67 eV; the contribution from process I peaks at $\sim$25 eV.

Earlier, Möhlmann et al. (1978) have measured the cross section of H, D Lyα by electron impact on HD for the energy range 100–2000 eV. Their cross section value at 100 eV is 10.8×10^{-18} cm^2 compared to our value of 7.98×10^{-18} cm^2. The H, D Lyα cross sections of Möhlmann et al. (1978), however, need to be corrected. The reason is that Möhlmann et al. (1978) used the measured H Lyα (from H_2) cross section value of 12.0×10^{-18} cm^2 at 100 eV to obtain their H, D Lyα cross section (from HD); while in the present study we have used the recently measured value of 7.6×10^{-18} cm^2 from Liu et al. (1998) for the H Lyα (from H_2), which is more accurate. To test this proposition, we normalized the H, D Lyα value of Möhlmann

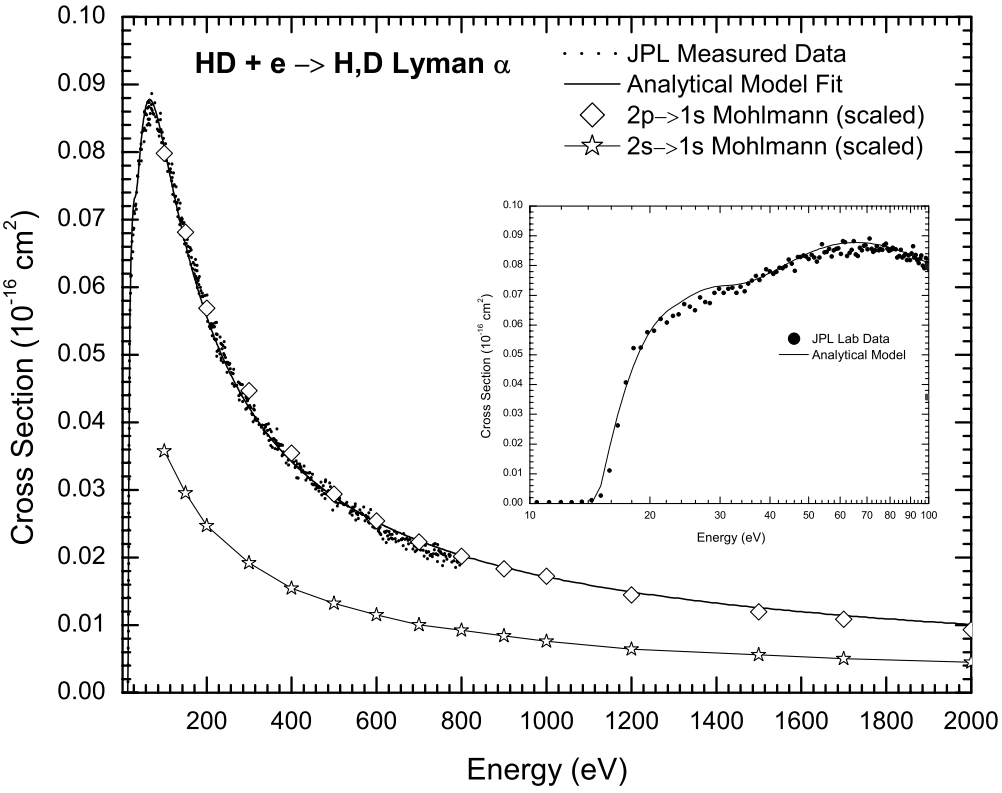

Fig. 3.—Total H, D Lyα model cross section compared with the experimental excitation function in the 0–800 eV energy range. The FWHM was 0.8 Å centered at 1215.5 Å. The experimental excitation function data of Möhlmann et al. (1978) for H, D (2p) and H, D (2s) states from 100 to 2000 eV are shown after a normalization (see text). The inset shows the comparison between experimental excitation function and model in the near threshold and low-energy region. Note that the energy in inset is in logarithmic scale. The model parameters are given in Table 2. The cross section was measured in the static gas mode.

TABLE 3
Cross Sections for the H, D Lyα

Electron Energy (eV)	Cross Section (10^{-18} cm^2)
15	0.2
17.5	4.0
20	5.7
25	6.6
30	7.1
40	7.8
50	8.3
60	8.5
70	8.6
80	8.5
90	8.2
100	8.0
125	7.3
150	6.7
175	6.0
200	5.6
225	5.2
250	4.8
275	4.4
300	4.2
350	3.7
400	3.4
450	3.1
500	2.8
550	2.6
600	2.4
650	2.3
700	2.1
750	2.1
800	2.0
900	1.8
1000	1.7
1100	1.5
1300	1.4
1500	1.2
1750	1.0
2000	0.96

et al. (1978) at 100 eV with our measured value and apply this correction to their H, D Lyα cross sections at all energies. The resulting cross section values are shown in Figure 3 with diamonds. The agreement between the two measurements is good over the overlapping energy range of 100–800 eV.

Having established the consistency between our measured H, D Lyα values with those of Möhlmann et al. (1978), after applying correction, we can compare the results of the analytical model to the data of Möhlmann et al. (1978) for obtaining a verification of the predicted cross section at higher energies. The model cross sections extending to 2 keV are also plotted in Figure 3, which shows that the analytical model cross sections are consistent with the corrected values of Möhlmann et al. (1978). At higher (above 1 keV) energies, the H, D Lyα cross section is dominated by the singlet-states, which follow the asymptotic Born dipole shape predicted by the model. Table 3 presents the cross sections for H, D Lyα at selected energies from threshold to 2 keV; the values have an estimated error of about 15%.

8. DISCUSSION

We have contributed significantly to the molecular physics database for HD through the process of analyzing a high-resolution ultraviolet emission spectrum of molecular deuterium hydride excited by electron impact at 100 eV under optically thin, single-scattering experimental conditions. The analysis of the spectrum is based upon newly calculated transition probabilities and line positions with rovibrational coupling for the strongest ($n = 2$ and 3) band systems, $B\ ^1\Sigma_u^+$–$X\ ^1\Sigma_g^+$, $B'\ ^1\Sigma_u^+$–$X\ ^1\Sigma_g^+$, $C\ ^1\Pi_u$–$X\ ^1\Sigma_g^+$, and $D\ ^1\Pi_u$–$X\ ^1\Sigma_g^+$. The high-resolution laboratory spectrum (FWHM = 160 mÅ) covers the wavelength range from 900 to 1650 Å, and contains the two Rydberg series of HD: $^1\Sigma_u^+ 1s\sigma np\sigma$ (B, B', B'', $n = 2, 3, 4$) $\rightarrow X\ ^1\Sigma_g^+$ and $^1\Pi_u^+ 1s\sigma np\pi$ (C, D, D', D'', $n = 2, 3, 4, 5$) $\rightarrow X\ ^1\Sigma_g^+$. A regression analysis of the experimental spectrum over the observed wavelength range using synthetic spectra for the $n = 2$ and 3 band systems of HD is in good agreement with observed intensities, showing minor contributions from the $n = 4$ and 5 members of the Rydberg series at wavelengths above 900 Å.

8.1. *Comparison with the Model Spectra*

We compare now the experimental and fitted spectra in the two selected spectral regions. These two narrow wavelength regions are shown in Figure 4 (*top and bottom panels*). The first region extends from 1350 to 1360 Å and includes the rotational lines from a strong cascade band $B(0, 5)$ [$B\ ^1\Sigma_u^+(v' = 0) \rightarrow X\ ^1\Sigma_g^+(v'' = 5)$]. The second region, 1380–1390 Å, lies between the B(0, 5) and B(0, 6) bands and therefore contains fewer contributions from the cascade excitation.

In the first spectral region, some peaks are found in the laboratory data, but they do not appear in the model. A careful inspection of Table 4 shows that the poor fit arises from transitions involving $v' = 0$ of the B upper state. This may be explained by the cascade mechanism: the electrons excite the g-states, like the EF state, whose near-infrared or visible emission populates principally the lower levels of the B state that subsequently fluoresce toward the ground rovibrational states. This effect appears also, but less strongly, for some peaks in the second spectral region between 1380 and 1390 Å.

In the second spectral region, some regions of the experimental spectrum have less intensity than the model. As the calculations do not take into account the coupling between the g and u states, this lack of agreement could be explained by the borrowing effect for mutually interacting electronic states.

Between 1384.5 and 1385 Å, the difference is nearly 50%. Inspection of Table 5 shows that the B, $v = 10$ rotational levels emit in this region and the rotational levels are perturbed by the EF state with $v = 2$. Dabrowski & Herzberg (1976) have measured a gap of 104.2 cm^{-1} between the $v = 2$ level for $J = 1$; $o - c$ (observed − calculated) of Table 5 is 0.033 Å (1.7 cm^{-1}) close to the shift due to the g-u coupling. If we use the two-level coupling approximation, the intensity loss due to the perturbation is 1.7/104.2. This amount is too small to explain the discrepancy, even if we take into account the cascade de-excitation path due to g-u coupling.

Between 1387 and 1390 Å, the experimental structures are only slightly lower than the model. Table 4 shows that rotational levels of the B, $v = 12$ emit in this region. Hinnen et al. (1995) has studied its perturbation by the EF, $v = 5$; for $J = 3$, the gap between the two g and u states is 30.8 cm^{-1} and $o - c$ of Table 5 is close to 3 cm^{-1}, this is compatible with the borrowing effect.

We have made a major effort to explain these discrepancies. We show in Figure 5 a regression fit of the data in the same two FUV spectral regions as in Figure 4 by a model that consists of direct excitation of the Lyman band system and cascading by the EF intermediate state. The EF–B cascade is the strongest

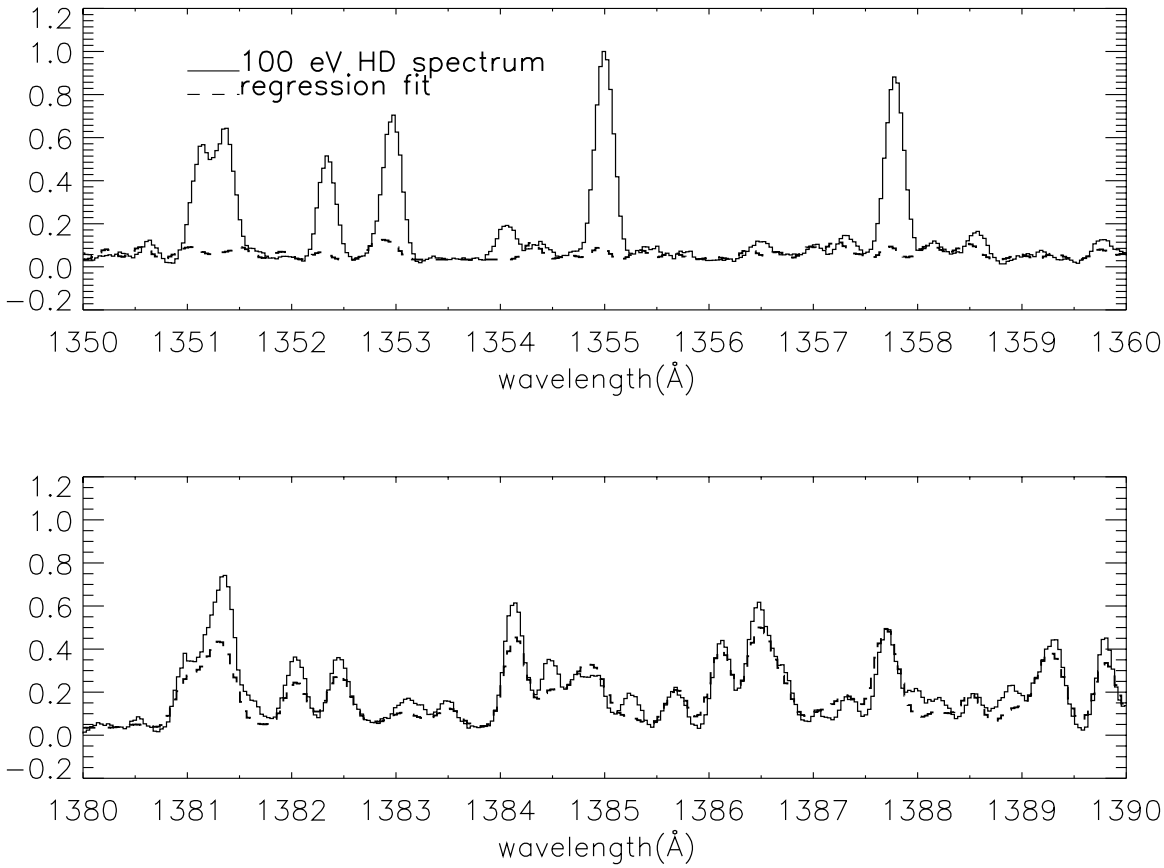

FIG. 4.—Comparison between the experimental spectrum (*solid lines*) and a model synthetic spectrum (*dashed lines*) based on the regression analysis obtained at 300 K gas temperature, 100 eV electron impact energy, and 0.160 Å FWHM from 1350 to 1360 Å in the top panel and 1380 to 1390 Å in the bottom panel, as described in the figure caption to Fig. 2.

intermediate g-state that contributes to cascading. We have calculated transition probabilities of the $EF\ ^1\Sigma_g^+ - B\ ^1\Sigma_u^+$ band system by using the electronic factor of excitation shape function *X-EF* obtained for H_2 by Liu et al. (2003) and the vibrational wave function of HD. The regression model is in excellent agreement with the observed data, proving cascade emission is easily observable in the FUV. As we have shown for H_2 (Liu et al. 2002) many cascade channels from the *EF* state contribute to each cascade contribution to a rotational line. Other gerade Rydberg series members contribute to this spectrum including the *GK*, $H\hat{H}$, *I*, *J*, . . . , states, although the *EF* state remains the strongest contributor. Consideration of only the *EF* state will slightly underestimate the observed intensity.

8.2. *Cross Sections*

Although there have been previous high-resolution spectral emission studies of H Lyα and D Lyα line profiles and cross section studies from H_2 and D_2, respectively, by our laboratory program at JPL (cf. Ajello et al. 2003), the measurements presented here are the first conducted upon HD. The most recent review of electron-molecule collision by Compton & Bardsley (1984) indicates two emission cross section studies of HD in the past: (1) by Möhlmann et al. (1978) to study the H, D Lyα emission cross sections from dissociative excitation of HD, and (2) by Karolis & Harting (1978) to determine the Balmer series emission cross sections also from dissociative excitation of HD.

From earlier studies by the Dutch group it is known that in case of electron impact dissociative excitation of H_2 and D_2, a considerable fraction of the produced H and D atoms in the $n = 2$ are in the 2s state. However, for some H-containing molecules, like H_2O, NH_3, CH_4, and HCl, no H atom in the 2s state is produced in the dissociation excitation by electron impact. Möhlmann et al. (1978) have measured the H, D ($2s \rightarrow 1s$) cross sections at energies 100 eV to 2 keV for electron impact dissociative excitation of HD. Their measured value at 100 eV is 4.84×10^{-18} cm^2. As in the case of the H, D Lyα (i.e., $2p \rightarrow 1s$ transition) cross section (discussed in § 7), we can correct their H, D (2s) cross sections by normalizing them with the ratio 7.98/10.8 for the H, D ($2p \rightarrow 1s$) cross section at 100 eV. This scaling gives a cross section value of 3.58×10^{-18} cm^2 for the H, D (2s) production in electron impact on HD. The scaled H, D ($2s \rightarrow 1s$) cross section values of Möhlmann et al. (1978) are also shown in Figure 3 (line with open star). Thus, the total cross section for the H, D ($2p$, $2s \rightarrow 1s$) emission at 100 eV would be $(7.98 + 3.58) \times 10^{-18} = 1.16 \times 10^{-17}$ cm^2. It is interesting to note, as quoted by Möhlmann et al. (1978), that only in the cases (i.e., H_2, HD, and D_2) in which the minimum required energy to produce the H ($n = 2$) is smaller than the ionization potential of the parent molecules, that the H(2s) atoms are produced.

The ratio of the emission cross sections for the production of H(2s) to that of H(2p) [i.e., H, D (2s/2p) ratio], produced in e + HD at 100 eV, as given by Möhlmann et al. (1978), is 0.448, and it remains roughly constant (between 0.43 and 0.49) throughout the energy range 100–2000 eV. The H, D (2s/2p) ratio value for H_2 of Möhlmann et al. is 0.605, which is comparable to the value is 0.697 obtained by Ajello et al. (1991). The Lyman band and Werner band direct cross sections at 100 eV for HD and H_2 can also be compared. The Lyman and Werner cross sections for

TABLE 4

CALCULATED TRANSITION WAVELENGTHS AND EMISSION TRANSITION PROBABILITIES BETWEEN 1350 AND 1357 Å

Transition	λ (Å)	$o-c$ (Å)	A (s^{-1})
B 3–6 *P*4	1350.098	0.017	4.66E+06
B 20–14 *R*1	1350.233	...	2.57E+06
B 20–14 *R*0	1350.241	...	2.29E+06
B 13–10 *P*6	1350.253	...	1.85E+07
C 6–16 *R*4	1350.417	...	2.34E+05
B 20–14 *R*2	1350.496	...	2.62E+06
B 17–12 *P*5	1350.530	...	1.28E+07
B 5–7 *R*2	1350.607	0.020	9.90E+06
B 19–13 *P*6	1350.876	...	1.12E+07
B 5–7 *P*1	1350.953	0.024	1.49E+07
B 10–9 *R*4	1350.987	...	2.78E+05
B 20–14 *R*3	1350.990	...	2.62E+06
B 20–14 *P*1	1351.086	...	8.24E+06
B 0–5 *R*0	1351.107	0.008	1.44E+08
B 0–5 *R*1	1351.323	0.012	1.74E+08
B 10–9 *P*3	1351.505	...	3.66E+06
B 12–10 *R*0	1351.508	...	4.26E+05
B 8–8 *P*5	1351.621	...	7.86E+06
B 20–14 *R*4	1351.630	...	2.36E+06
B 12–10 *R*1	1351.732	...	3.52E+05
C 6–16 *Q*5	1351.902	...	2.82E+04
B 20–14 *P*2	1351.921	...	6.09E+06
B 22–16 *R*3	1352.010	...	1.16E+06
B 22–16 *R*4	1352.238	...	2.08E+06
B 5–7 *R*3	1352.280	0.031	1.15E+07
B 0–5 *R*2	1352.300	0.011	1.87E+08
B 12–10 *R*2	1352.536	...	2.50E+05
B 22–16 *R*2	1352.539	...	1.41E+06
B 12–10 *P*1	1352.798	...	2.43E+06
B 5–7 *P*2	1352.809	0.023	8.95E+06
B 22–16 *R*1	1352.837	...	1.30E+06
B 0–5 *P*1	1352.928	0.012	4.29E+08
B 15–11 *P*6	1352.973	...	1.53E+07
B 20–14 *P*3	1352.999	...	6.06E+06
C 6–16 *R*3	1353.088	...	5.99E+05
B 22–16 *R*0	1353.107	...	1.11E+06
B 17–12 *P*6	1353.325	...	1.32E+07
C 5–14 *R*4	1353.502	...	5.16E+05
B 22–16 *P*1	1353.660	...	4.06E+06
C 6–16 *Q*4	1353.855	...	2.79E+04
B 12–10 *R*3	1353.900	...	1.63E+05
B 22–16 *P*2	1353.936	...	3.15E+06
B 0–5 *R*3	1354.023	0.011	1.94E+08
B 22–16 *P*5	1354.061	...	3.51E+06
B 3–6 *P*5	1354.150	...	4.35E+06
B 22–16 *P*3	1354.167	...	3.37E+06
B 21–15 *R*1	1354.290	...	1.37E+06
B 22–16 *P*4	1354.291	...	3.89E+06
B 20–14 *P*4	1354.303	...	6.32E+06
B 12–10 *P*2	1354.311	...	2.15E+06
B 10–9 *P*4	1354.341	...	4.14E+06
B 21–15 *R*2	1354.342	...	1.42E+06
B 21–15 *R*0	1354.396	...	1.21E+06
C 5–14 *R*3	1354.477	...	1.30E+05
B 21–15 *R*3	1354.524	...	1.50E+06
C 6–16 *R*2	1354.548	...	6.28E+04
B 5–7 *R*4	1354.641	...	1.31E+07
B 18–13 *R*0	1354.649	...	1.36E+06
B 18–13 *R*1	1354.727	...	1.44E+06
B 21–15 *R*4	1354.812	...	1.62E+06
B 14–11 *R*0	1354.874	...	4.16E+05
B 0–5 *P*2	1354.969	0.010	2.85E+08
B 14–11 *R*1	1355.060	...	3.59E+05
B 21–15 *P*1	1355.106	...	4.62E+06
C 6–16 *P*5	1355.143	...	2.24E+06
B 18–13 *R*2	1355.163	...	1.41E+06
C 6–16 *Q*3	1355.339	...	2.56E+04
B 5–7 *P*3	1355.355	0.026	7.33E+06
C 5–14 *R*2	1355.437	...	4.27E+04
B 18–13 *P*1	1355.631	...	5.54E+06
B 21–15 *P*2	1355.702	...	3.56E+06
B 14–11 *R*2	1355.764	...	2.77E+05
B 20–14 *P*5	1355.777	...	6.52E+06
B 12–10 *R*4	1355.814	...	1.00E+05
C 6–16 *R*1	1355.844	...	6.35E+03
B 8–8 *P*6	1355.854	...	8.34E+06
B 18–13 *R*3	1355.949	...	1.38E+06
B 16–12 *R*0	1356.045	...	7.04E+05
B 14–11 *P*1	1356.070	...	2.34E+06
C 5–14 *Q*5	1356.142	...	2.94E+04
B 16–12 *R*1	1356.180	...	6.84E+05
C 6–16 *P*4	1356.306	...	3.57E+05
C 5–14 *R*1	1356.307	...	9.63E+03
B 12–10 *P*3	1356.382	...	2.50E+06
C 6–16 *Q*2	1356.416	...	2.32E+04
B 21–15 *P*3	1356.427	...	3.68E+06
B 0–5 *R*4	1356.490	0.010	1.99E+08
B 18–13 *P*2	1356.669	...	4.38E+06
C 5–14 *Q*4	1356.731	...	2.35E+04
B 16–12 *R*2	1356.765	...	6.13E+05
C 6–16 *R*0	1356.822	...	6.62E+02
B 22–17 *R*1	1356.874	...	4.10E+06
B 14–11 *R*3	1356.971	...	2.11E+05
B 7–8 *R*0	1356.982	0.029	6.56E+06
B 18–13 *R*4	1357.058	...	1.37E+06
C 5–14 *R*0	1357.090	...	7.52E–01
C 6–16 *Q*1	1357.113	...	2.14E+04
B 16–12 *P*1	1357.137	...	3.38E+06
C 5–14 *Q*3	1357.167	...	1.91E+04
C 6–16 *P*3	1357.180	...	1.20E+05
B 7–8 *R*1	1357.238	0.029	8.68E+06
B 21–15 *P*4	1357.254	...	4.00E+06
B 20–14 *P*6	1357.307	...	5.94E+06
B 22–17 *R*0	1357.341	...	3.64E+06
B 14–11 *P*2	1357.447	...	2.09E+06
C 5–14 *Q*2	1357.478	...	1.60E+04
C 6–16 *P*2	1357.656	...	4.67E+04
C 5–14 *Q*1	1357.671	...	1.40E+04
B 22–17 *P*1	1357.702	...	6.44E+06
B 0–5 *P*3	1357.744	0.012	2.55E+08
B 10–9 *P*5	1357.745	...	4.70E+06
B 16–12 *R*3	1357.783	...	5.55E+05

TABLE 5

CALCULATED TRANSITION WAVELENGTHS AND EMISSION TRANSITION PROBABILITIES BETWEEN 1380 AND 1390 Å

Transition	λ (Å)	$o-c$ (Å)	A (s^{-1})
C 2–11 *P*6	1380.020	...	2.05E+05
B 13–11 *P*5	1380.189	...	6.32E+05
B 19–15 *R*1	1380.229	...	8.69E+05
B 19–15 *R*2	1380.234	...	9.10E+05
B 19–15 *R*3	1380.357	...	8.37E+05
B 19–15 *R*0	1380.371	...	6.76E+05
B 6–8 *R*4	1380.460	0.027	4.67E+07
B 19–15 *R*4	1380.573	...	6.75E+05
C 0–9 *P*5	1380.750	...	1.44E+04
C 1–10 *P*5	1380.843	...	1.40E+03
C 5–16 *R*3	1380.900	...	5.99E+04
B 8–9 *R*0	1380.932	0.031	2.52E+07
B 18–14 *P*4	1380.962	...	1.70E+04
B 19–15 *P*1	1381.124	...	1.24E+06
B 8–9 *R*1	1381.149	0.033	3.07E+07
B 6–8 *P*3	1381.316	0.029	5.53E+07
B 1–6 *R*0	1381.396	0.016	2.54E+07
B 1–6 *R*1	1381.603	0.015	2.89E+07
B 19–15 *P*2	1381.728	...	4.87E+05
B 11–10 *P*6	1381.778	...	1.50E+06
B 4–7 *P*5	1381.928	0.023	6.78E+07
C 5–16 *Q*4	1382.002	...	8.59E+00
B 8–9 *R*2	1382.002	0.032	3.33E+07
B 15–12 *P*6	1382.122	...	5.76E+04
B 20–17 *R*1	1382.173	...	6.23E+06
B 8–9 *P*1	1382.407	0.032	7.26E+07
C 0–9 *P*6	1382.448	...	6.32E+03
B 19–15 *P*3	1382.449	...	1.69E+05
B 18–14 *P*5	1382.450	...	3.02E+04
C 1–10 *P*6	1382.550	...	4.95E+05
B 1–6 *R*2	1382.555	0.013	2.91E+07
B 20–17 *R*0	1382.679	...	6.00E+06
C 5–16 *R*2	1382.806	...	3.68E+04
B 16–13 *R*0	1382.959	...	3.72E+06
B 16–13 *R*1	1383.004	...	4.73E+06
C 5–16 *P*5	1383.040	...	2.26E+05
B 20–17 *P*1	1383.067	...	9.64E+06
C 4–14 *R*4	1383.137	...	7.85E+04
B 1–6 *P*1	1383.208	0.014	8.22E+07
B 19–15 *P*4	1383.258	...	1.22E+04
B 13–11 *P*6	1383.391	...	3.64E+05
B 16–13 *R*2	1383.407	...	5.21E+06
B 8–9 *R*3	1383.475	0.033	3.48E+07
C 5–16 *Q*3	1383.696	...	6.53E+01
B 16–13 *P*1	1383.999	...	9.00E+06
B 18–14 *P*6	1384.059	...	2.36E+05
B 8–9 *P*2	1384.096	0.030	4.72E+07
B 19–15 *P*5	1384.103	...	4.68E+04
B 16–13 *R*3	1384.160	...	5.40E+06
B 1–6 *R*3	1384.239	0.017	2.79E+07
C 5–16 *R*1	1384.312	...	2.14E+04
B 6–8 *P*4	1384.423	0.025	5.17E+07
C 4–14 *R*3	1384.449	...	9.35E+04
C 5–16 *P*4	1384.637	...	8.18E+04
B 10–10 *R*0	1384.679	0.033	1.89E+07
B 10–10 *R*1	1384.868	0.036	2.32E+07
B 19–15 *P*6	1384.926	...	3.26E+05

TABLE 5—*Continued*

Transition	λ (Å)	$o-c$ (Å)	A (s^{-1})
C 5–16 *Q*2	1384.930	...	1.35E+02
B 16–13 *P*2	1385.063	...	5.05E+06
B 1–6 *P*2	1385.223	0.012	5.61E+07
B 16–13 *R*4	1385.244	...	5.38E+06
C 5–16 *R*0	1385.423	...	8.09E+03
B 8–9 *R*4	1385.559	0.033	3.59E+07
C 4–14 *R*2	1385.629	...	8.95E+04
B 10–10 *R*2	1385.643	0.034	2.52E+07
C 5–16 *P*3	1385.704	...	3.56E+04
C 5–16 *Q*1	1385.732	...	1.91E+02
B 14–12 *R*0	1386.033	...	8.22E+06
B 10–10 *P*1	1386.056	0.033	5.38E+07
C 4–14 *Q*5	1386.062	...	4.08E+02
B 14–12 *R*1	1386.136	...	1.02E+07
C 5–16 *P*2	1386.291	...	1.23E+04
B 8–9 *P*3	1386.400	0.032	4.13E+07
B 16–13 *P*3	1386.477	...	3.60E+06
B 12–11 *R*0	1386.483	0.045	1.34E+07
B 4–7 *P*6	1386.506	0.022	6.58E+07
B 12–11 *R*1	1386.636	0.049	1.65E+07
B 1–6 *R*4	1386.652	0.015	2.62E+07
C 4–14 *R*1	1386.663	...	6.68E+04
B 14–12 *R*2	1386.690	...	1.12E+07
C 4–14 *Q*4	1386.862	...	5.44E+02
B 10–10 *R*3	1386.985	0.038	2.64E+07
B 14–12 *P*1	1387.193	...	2.18E+07
B 12–11 *R*2	1387.311	0.055	1.80E+07
C 4–14 *Q*3	1387.465	...	6.46E+02
C 4–14 *R*0	1387.565	...	2.96E+04
B 10–10 *P*2	1387.621	0.042	3.46E+07
B 14–12 *R*3	1387.678	...	1.17E+07
B 12–11 *P*1	1387.757	0.043	3.71E+07
C 4–14 *Q*2	1387.903	...	7.16E+02
B 1–6 *P*3	1387.961	0.015	5.11E+07
B 6–8 *P*5	1388.151	0.028	4.92E+07
C 4–14 *Q*1	1388.179	...	7.58E+02
B 16–13 *P*4	1388.217	...	2.51E+06
B 14–12 *P*2	1388.451	...	1.33E+07
B 12–11 *R*3	1388.492	0.005	1.88E+07
C 5–17 *R*1	1388.539	...	1.60E+04
B 3–7 *R*0	1388.849	0.019	2.58E+07
B 10–10 *R*4	1388.882	0.038	2.72E+07
B 3–7 *R*1	1389.066	0.022	2.95E+07
C 4–14 *P*6	1389.082	...	1.72E+05
B 14–12 *R*4	1389.083	...	1.19E+07
B 12–11 *P*2	1389.178	0.046	2.34E+07
B 8–9 *P*4	1389.308	0.033	3.82E+07
C 4–14 *P*2	1389.339	...	3.55E+04
C 4–14 *P*5	1389.476	...	1.25E+05
C 4–14 *P*3	1389.581	...	7.10E+04
C 4–14 *P*4	1389.636	...	9.82E+04
B 10–10 *P*3	1389.750	0.037	2.99E+07
C 5–17 *R*0	1389.861	...	4.58E+03
C 5–17 *Q*1	1389.968	...	1.51E+01
B 3–7 *R*2	1390.003	0.019	3.00E+07

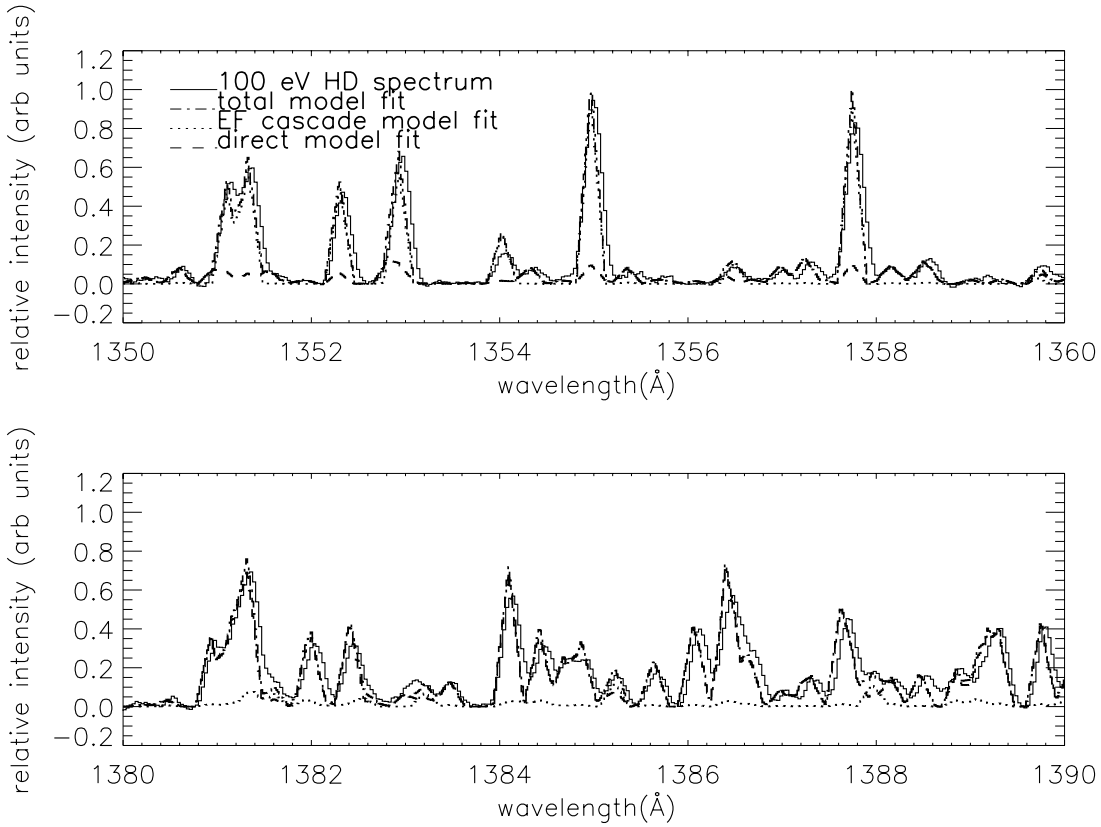

FIG. 5.—Comparison between the experimental spectrum (*solid lines*) and a model synthetic spectrum (*dash-dotted lines*) based on a second regression analysis. The second regression analysis includes contribution from both direct excitation of the $B\ ^1\Sigma_u^+$ state from the ground state (*dashed lines*) and cascade excitation from the process $X\ ^1\Sigma_g \rightarrow EF\ ^1\Sigma_g^+ \rightarrow B\ ^1\Sigma_u^+$ calculated by using the H_2 experimental shape function of Liu et al. (2003) but the vibrational wave functions of HD (*dotted lines*). We assume a 300 K gas temperature, 100 eV electron impact energy, and 0.160 Å FWHM, from 1350 to 1360 Å in the top panel and 1380 to 1390 Å in the bottom panel.

HD are 2.57×10^{-17} and 2.54×10^{-17} cm^2, respectively, while for H_2 these values are 2.62×10^{-17} and 2.40×10^{-17} cm^2, respectively (Liu et al. 1998). The ratio of Lyman (*B*-state) to Werner (*C*-state) cross sections at 100 eV is 1.01 and 1.09 for HD and H_2, respectively (cf. Table 1). The absolute Lyman and Werner cross sections for D_2 are nearly the same as for H_2, based on the assumption by Abgrall et al. (1999) that the Lyman and Werner band excitation shape functions are the same for H_2 and D_2. In this experiment the estimated uncertainties to both the Lyman and Werner band system 100 eV direct excitation cross sections from HD are 10%, whereas the estimated uncertainties to both the $B'-X$ and $D-X$ band system 100 eV direct excitation cross sections are 25%.

We now have completed the high-resolution spectroscopic laboratory studies of the hydrogen isotopomers, H_2, HD, and D_2 by electron impact under optically thin conditions: leading to a fundamental set of molecular emission and excitation cross sections and a verification of the ab initio calculations of transition probabilities for $n = 2$ and 3 gerade Rydberg series members. The results of this laboratory program are amenable to calculation of synthetic model spectra and electron energy loss processes in planetary atmospheres, cometary atmospheres, stellar atmospheres, and the ISM involving collisions of electrons with hydrogenic molecules.

The laboratory measurements described in this text was carried out at the Jet Propulsion Laboratory, California Institute of Technology. The work was supported by the Aeronomy Program of the National Science Foundation Program (grant ATM 03-1210), and NASA Planetary Atmospheres and NASA Astronomy and Physics Research Analysis Program Offices. P. Vatti Palle acknowledges the support of a National Research Council Resident Research Associateship while at the Jet Propulsion Laboratory. A part of this research was conducted while A. Bhardwaj held the National Research Council Resident Senior Research Associateship at NASA Marshall Space Flight Center.

REFERENCES

Abgrall, H., Roueff, E., & Drira, I. 2000, A&AS, 141, 297
Abgrall, H., Roueff, E., Launay, F., & Roncin, J. Y. 1994, Canadian J. Phys., 72, 856
Abgrall, H., Roueff, E., Launay, F., Roncin, J. Y., & Subtil, J. L. 1993a, A&AS, 101, 273
———. 1993b, A&AS, 101, 323
———. 1993c, J. Mol. Spectrosc., 157, 512
Abgrall, H., Roueff, E., Liu, X., & Shemansky, D. E. 1997, ApJ, 481, 557
Abgrall, H., Roueff, E., Liu, X., Shemansky, D. E., & James, G. K. 1999, J. Phys. B, 32, 3813
Ajello, J. M., Ahmed, S. M., Kanik, I., & Multari, R. 1995a, Phys. Rev. Lett., 75, 3261
Ajello, J. M., Ahmed, S., & Liu, X. 1996, Phys. Rev. A, 53, 2303
Ajello, J. M., James, G., Franklin, B., & Howell, S. 1990, J. Phys. B, 23, 4355
Ajello, J. M., James, G. K., & Shemansky, D. E. 1991, ApJ, 371, 422
Ajello, J. M., Kanik, I., Ahmed, S. M., & Clarke, J. 1995b, J. Geophys. Res., 100, 411
Ajello, J., Pryor, W., Esposito, L., Stewart, I., McClintock, W., Gustin, J., Grodent, D., Gerard, J.-C., & Clarke, J. T. 2005, Icarus, in press
Ajello, J., Shemansky, D. E., Pryor, W. R., Stewart, A. I., Simmons, K. E., Majeed, T., Waite, J. H., Gladstone, G. R., & Grodent, D. 2001, Icarus, 152, 151

Ajello, J., Vatti Palle, P., & Osinski, G. 2003, in Current Developments in Atomic, Molecular Physics, ed. M. Mohan (New York: Academic Press), 143
Ajello, J. M., et al. 1988, Appl. Opt., 27, 890
———. 1998, J. Geophys. Res., 103, 125
Allison, A. C., & Dalgarno, A. 1970, At. Data, 1, 289
Amitay, Z., et al. 1999, Phys. Rev. A, 60, 3769
André M. K., et al. 2004, A&A, 422, 483
Ben Jaffel, L., Vidal-Madjar, A., Gladstone, G. R., McConnell, J. C., Emerich, C., Prangé, R., & Clarke, J. T. 1998, in ASP Conf. Ser. 143, The Scientific Impact of the Goddard High Resolution Spectrograph, ed. J. C. Brandt, T. B. Ake, & C. C. Petersen (San Francisco: ASP), 366
Bhardwaj, A. 1999, J. Geophys. Res., 104, 1929
———. 2003, Geophys. Res. Lett., 30, 2244
Bhardwaj, A., & Gladstone, G. R. 2000, Rev. Geophys., 38, 295
Bhardwaj, A., & Michael, M. 1999a, J. Geophys. Res., 104, 24713
———. 1999b, Geophys. Res. Lett., 26, 393
Bockelée-Morvan, D., Crovisier, J., Mumma, M. J., & Weaver, H. A. 2005, in in Comets II, ed. M. C. Festou, H. U. Keller, & H. A. Weaver (Tucson: Univ. Arizona Press), in press
Boissé, P., Le Petit, F., Rollinde, E., Roueff, E., Pineau des Forêts, G., Anderson, B.-G., Gry, C., & Felenbok, P. 2005, A&A, 429, 509
Celiberto, R., Janev, R. K., Laricchuta, A., Capitelli, M., Wadhera, J. M., & Atems, D. E. 2001, At. Data Nucl. Data Tables, 77, 161
Compton, R. N., & Bardsley, J. N. 1984, in Electron-Molecule Collisions ed. I. Shimamura & K. Takayanagi (New York: Plenum Press), 275
Dabrowski, I., & Herzberg, G. 1976, Canadian J. Phys., 54, 525
Dalgarno, A., Yan, M., & Liu, W. 1999, ApJS, 125, 237
Dehmer, P. M., & Chupka, W. A. 1983, J. Chem. Phys., 79, 1569
Dziczek, D., Ajello, J. M., James, G. K., & Hansen, D. L. 2000, Phys. Rev., 61, 064702
Ferlet, R., et al. 2000, ApJ, 538, L69
Furlong, J. M., & Newell, W. R. 1995, J. Phys. B, 28, 1851
Geiger, J., & Schmoranzer, H. 1969, J. Mol. Spectrosc., 32, 39
Hara, S. 1971, J. Phys. Soc. Japan, 30, 819
Hinnen, P. C., Werners, S. E., Hogervorst, W., Stolte, S., & Ubachs, W. 1995, Phys. Rev. A, 52, 4425
Jackman, C. H., Garvey, R. H., & Green, A. E. S. 1977, J. Geophys. Res., 82, 5081
Jonin, C., Liu, X. Ajello, J. M., James, G. K., & Abgrall, H. 2000, ApJS, 129, 247
Karolis, C., & Harting, E. 1978, J. Phys. B, 11, 357
Kazanskii, A. K. 1996, Opt. Spectrosc., 80, 798
Kolos, W., & Wolniewicz, I. 1969, J. Chem. Phys., 50, 3228
Lacour, S., et al. 2005, A&A, 430, 967
Liu, X., Ahmed, S. M., Multari, R. A., James, G. K., & Ajello, J. M. 1995, ApJS, 101, 375
Liu, X., Shemansky, D. E., Abgrall, H., Roueff, E., Dziczek, D., Hansen, D. L., & Ajello, J. M. 2002, ApJS, 138, 229
Liu, X., Shemansky, D. E., Ahmed, S., Ajello, J., Abgrall, H., & Roueff, E. 2003, J. Phys. B, 36, 173
Liu, X., Shemansky, D. E., Ahmed, S. M., James, G. K., & Ajello, J. M. 1998, J. Geophys. Res., 103, 739
Liu, X., Shemansky, D., Ajello, J., James, G., & Abgrall, H. 2000, ApJS, 129, 267
Möhlmann, G. R., Shima, K. H., & de Heer, F. J. 1978, J. Chem. Phys., 28, 333
Morton, D. 1975, ApJ, 197, 85
Parkinson, C. D., Griffioen, E., McConnell, J. C., Ben Jaffel, L., Vidal-Madjar, A., Clarke, J. T., & Gladstone, G. R. 1999, Geophys. Res. Lett., 26, 3177
Senn, P., Quadrelli, P., & Dressler, K. 1988, J. Chem. Phys., 89, 7401
Singhal, R. P., Chakravarty, S. C., Bhardwaj, A., & Prasad, B. 1992, J. Geophys. Res., 97, 18245
Spitzer, L., Drake, J. F., Jenkins, E. B., Morton, D. C., Rogerson, J. B., & York, D. G. 1973, ApJ, 181, L116
Staszewska, G., & Wolniewicz, L. 2002, J. Mol. Spectrosc., 212, 208
Taylor, F. W., Atreya, S. K., Encrenaz, T., Hunten, D. H., Irwin, P. G., & Owen, T. C. 2004, in Jupiter: The Atmosphere, Satellite and Magnetopshere, ed. F. Bagenal et al. (Cambridge: Cambridge Univ. Press), 59
Vatti Palle, P., Ajello, J., & Bhardwaj, A. 2004, J. Geophys. Res., 109, 02310
Vidal-Madjar, A., Lecavelier des Etangs, A., Désert, J.-M., Ballester, G. E., Ferlet, R., Hébrard, G., & Mayor, M. 2003, Nature, 422, 143
Wolniewicz, L. 1993, J. Chem. Phys., 99, 1851
Wolniewicz, L., & Dressler, K. 1988, J. Chem. Phys., 88, 3861
Wolniewicz, L., & Staszewska, G. J. 2003a, J. Mol. Spectrosc., 217, 181
———. 2003b, J. Mol. Spectrosc., 220, 45